CHAPTER 28

MEASURING RATES AND DATES: THE USE OF RADIOISOTOPES IN THE STUDY OF MARINE PROCESSES

INTRODUCTION

Most of the elements in seawater and the sediments have several stable and radioactive isotopes. The relative oceanic abundances of these isotopes have been used to study biological, geological, physical, and chemical processes. This approach has arguably been the most productive in furthering our understanding of the crustal-ocean factory. For example, the radioactive isotopes, or **radionuclides**, have been used to determine rates of processes, such as those of sedimentation, photosynthesis, and various types of water motion. The stable isotopes have been used to establish the timing and intensity of climate changes, the structure of food chains, and the fate of terrestrial organic matter in the marine environment. Indeed, many hypotheses and conclusions presented in previous chapters are based on isotopic data. Some of this supporting evidence is presented in this chapter, which deals with the radionuclides. The use of stable isotopes is discussed in the next chapter.

MECHANISMS OF RADIOACTIVE DECAY

Radioisotopes are atoms that spontaneously lose nuclear material at a fixed rate. This process is termed **radioactive decay** and is an example of a nuclear reaction. Atoms with unstable nuclei spontaneously undergo radioactive decay and thereby attain a greater measure of stability. Nonradioactive atoms will undergo nuclear reactions, such as fusion, only if energy is applied either in the form of electromagnetic radiation or by collision with an energized particle.

In unstable nuclei, the repulsive forces are stronger than the attractive ones. Most nuclear repulsion is caused by electrostatic interactions among the positively charged **protons**. Thus the addition of protons to a nucleus causes a net increase in the repulsive forces. This instability can be counterbalanced by the addition of **neutrons**, which increases the attractive forces. The relative number of neutrons required to achieve a stable nucleus is shown in Figure 28.1. The relative number of neutrons needed to achieve stability increases

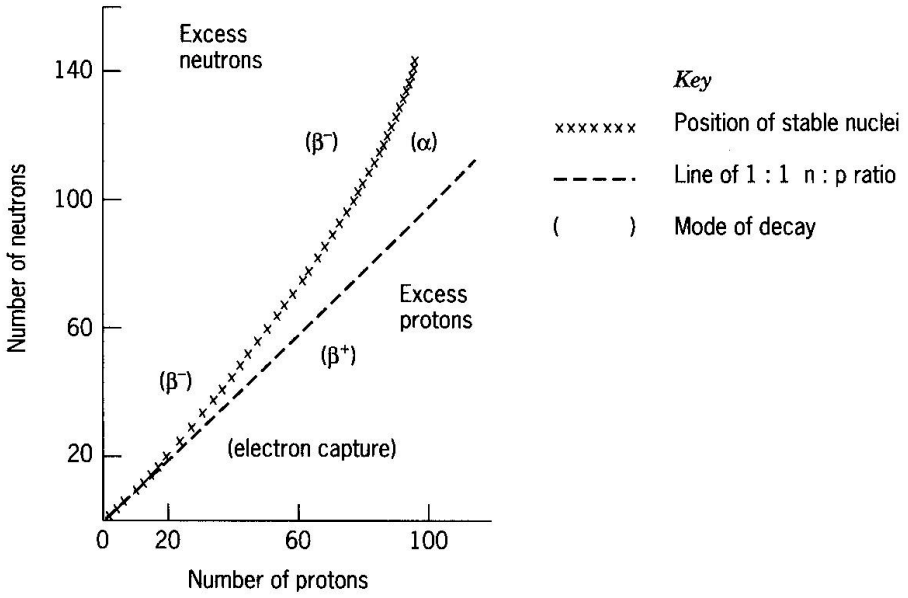

FIGURE 28.1. The neutron-to-proton ratio of radionuclides and its relationship to nuclear stability and radioactive-decay mechanisms.

with increasing mass number. Thus the neutron-to-proton ratio increases from 1:1 in the light nuclei ($Z \leq 17$) to 1.6:1 in the heavier elements. A nucleus with an excess of neutrons or protons spontaneously undergoes radioactive decay until a stable ratio is achieved. In many cases, this occurs through a series of radioactive decay steps, each of which progressively alters the neutron to proton ratio. Examples of such decay series are given later in this chapter.

If protons are in excess, stability is achieved either through emission of **α particles**, or positrons, or by electron capture. α particles are helium nuclei ($^4_2$He). Thus, their emission causes the radionuclide to lose two protons and two neutrons. This type of radioactive decay is characteristic of the larger radionuclides, as illustrated below:

$$^{238}_{92}\text{U} \rightarrow {}^{234}_{90}\text{Th} + {}^{4}_{2}\text{He} + Q \qquad (28.1)$$

Note that the neutron-to-proton ratio increases from 1.59 in the parent radionuclide, $^{238}_{92}$U, to 1.60 in its daughter isotope, $^{234}_{90}$Th. (Decay products are referred to as **daughters**.) Depending on the radionuclide, variable amounts of energy (Q) are released as gamma rays.

During positron emission, a proton spontaneously decomposes into a neutron and a positively charged particle ($^0_1$e) as follows:

$$^1_1p \rightarrow {}^1_0n + \beta^+(^0_1e) + Q \qquad (28.2)$$

Positrons are also called β^+ particles. They can be thought of as positively charged **electrons** and are destroyed as a result of collisions with electrons. Depending on the type of radionuclide undergoing positron emission, variable amounts of energy (Q) are released as neutrinos.

As shown in Figure 28.1, positron emission is characteristic of the radionuclides with intermediate atomic weights. These radionuclides are common products of nuclear reactions that occur in power plants and during detonation of atomic bombs. An example of positron emission is given below:

$$^{64}_{29}\text{Cu} \rightarrow {}^{64}_{28}\text{Ni} + {}^{0}_{1}e + Q \tag{28.3}$$

Note that the neutron-to-proton ratio of the nuclide increases from 1.21 to 1.29.

Excess protons are also destroyed through **electron capture**. In this reaction, an electron from the lowest energy level in the atom (1s) reacts with a proton, generating a neutron as illustrated below:

$$^{1}_{1}p + {}^{0}_{-1}e \rightarrow {}^{1}_{0}n \tag{28.4}$$

Due to their close proximity to the nucleus, the 1s electrons are most likely to be captured by the nucleus. They are replaced by higher-energy electrons. As these replacement electrons drop to the lower energy state, they emit short-wavelength radiation, called x-rays. This type of decay is characteristic of the low atomic weight isotopes.

^{40}K is unstable and spontaneously undergoes electron capture, as illustrated below:

$$^{40}_{19}\text{K} + {}^{-1}_{0}e \rightarrow {}^{40}_{18}\text{Ar} + Q \tag{28.5}$$

Only about 10 percent of ^{40}K decays by this mechanism. The majority (90%) decays to $^{40}_{20}$Ca via β^- emission. **β^- particles** are high-energy electrons ($^{0}_{-1}e$). Their emission from the nucleus causes a neutron to be converted to a proton. Thus radionuclides with an excess of neutrons decay via this process. As shown below, variable amounts of energy (Q) are also released, either in the form of neutrinos or gamma rays, depending on the radionuclide.

$$^{1}_{0}n \rightarrow {}^{1}_{1}p + \beta^-(^{0}_{-1}e) + Q \tag{28.6}$$

Tritium ($^{3}_{1}$H) also decays via β^- emission, as shown below:

$$^{3}_{1}\text{H} \rightarrow {}^{3}_{2}\text{He} + \beta^-(^{0}_{-1}e) + Q \tag{28.7}$$

RADIOACTIVE DECAY LAW

The rate at which a radionuclide decays is directly proportional to the number of atoms present; that is,

$$-\frac{dN}{dt} = \lambda N \tag{28.8}$$

where N, the number of atoms (e.g., moles or grams) of radionuclide N, decreases over time (t) as a result of radioactive decay. The rate constant, λ, is a characteristic of the radionuclide. It is a statistical measure of the likelihood for an average atom to undergo decay in a specified unit of time.

If the original and final numbers of atoms of the radionuclide are known, the amount of time over which radioactive decay has occurred can be inferred from the **radioactive decay law**. To do this, Eq. 28.8 must be integrated from the original time and number (t_o and N_o) to the final time and number (t_f and N_f) as follows:

$$\int_{N_o}^{N_f} \frac{1}{N} dN = -\lambda \int_{t_o}^{t_f} dt \tag{28.9}$$

The solution of this integral is

$$\ln N \Big|_{N_o}^{N_f} = -\lambda t \Big|_{t_o}^{t_f} \tag{28.10}$$

which can be rewritten as

$$\ln N_f - \ln N_o = -\lambda(t_f - t_o) \tag{28.11}$$

Substituting in $t_o = 0$, $t_f = t$ and $N_f = N$ yields

$$\ln(N/N_o) = -\lambda t \tag{28.12}$$

or

$$\frac{N}{N_o} = e^{-\lambda t} \tag{28.13}$$

Thus radioactive decay causes radionuclide numbers to decrease exponentially over time, as illustrated in Figure 28.2 for ^{14}C.

If half of N_o has decayed, then $N_f/N_o = 0.5$ and Eq. 28.13 becomes

$$0.5 = e^{-\lambda t_{\frac{1}{2}}} \tag{28.14}$$

where $t_{\frac{1}{2}}$ is the **half-life**. This can also be written as

$$\frac{0.693}{\lambda} = t_{\frac{1}{2}} \tag{28.15}$$

Since ^{14}C has a **decay constant** of 1.22×10^{-4}/y, its half-life is 5680 y.

CLASSIFICATION OF MARINE RADIONUCLIDES

Marine radionuclides are classified according to their source. Some of the atoms that coalesced to form this planet were radionuclides. Many of those with long half-lives are still present. The most abundant of these primordial radionuclides are ^{235}U, ^{238}U, and ^{232}Th, which have half-lives of 0.71, 4.5, and 14 billion years, respectively. Since the earth is 4.6 billion years old, 1.1 percent of the primordial ^{235}U is still present, while 49 percent and 80 percent of the ^{238}U and ^{232}Th remain. As shown in Figure 28.3, these isotopes decay through a series of steps and produce a variety of daughters whose half-lives range

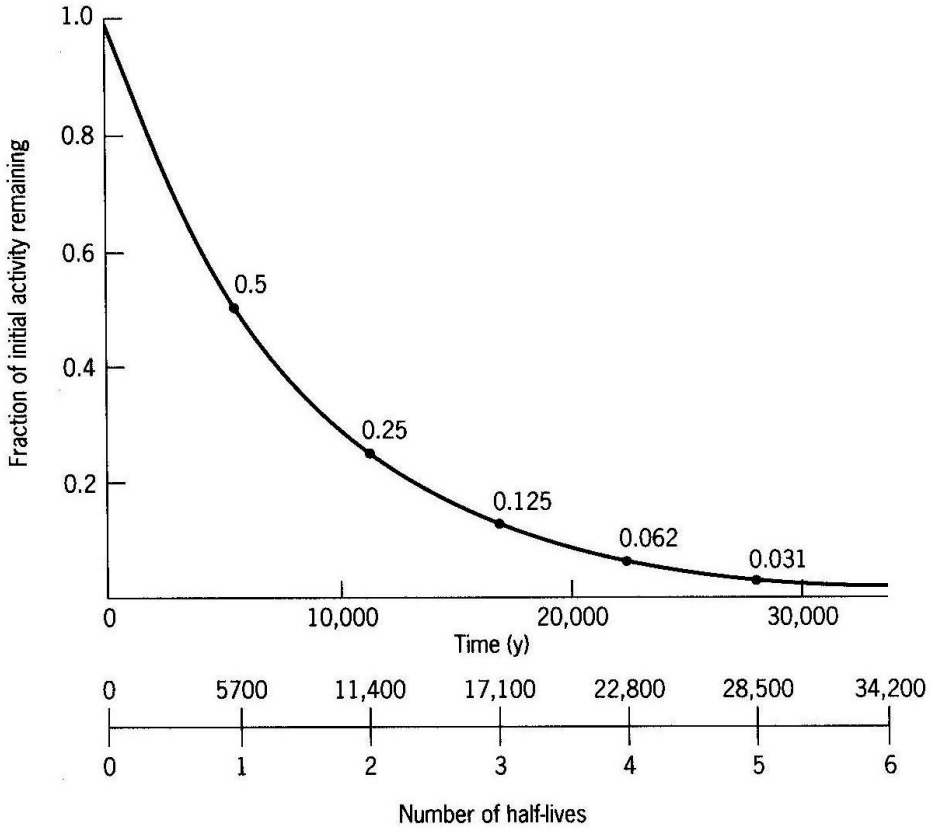

FIGURE 28.2. Exponential decline in the amount of ^{14}C as predicted by the radioactive decay law.

from fractions of seconds to thousands of years. The series end in stable isotopes of lead.

The primordial radionuclides decay by either α or β^- emission. The energy released during these nuclear reactions is partially dissipated as heat in the inner earth and makes a significant contribution to the geothermal gradient.

Cosmogenic radionuclides are formed by spallation reactions that occur in the atmosphere. In these reactions, gas nuclei are fragmented as a result of collisions with high-energy cosmic rays. Radiocarbon (^{14}C) is the cosmogenic radionuclide most commonly used by oceanographers. The artificial radionuclides are isotopes produced by humans. Most have been introduced into the ocean as a result of nuclear bomb testing and leakage from nuclear power plants. Due to differences in their sources and chemical behavior, the primordial, cosmogenic, and artificial radionuclides have distinct distributions and fates in the marine environment. As a result, they have proven useful for studying a multitude of marine processes. Some examples are described below.

THE PRIMORDIAL RADIONUCLIDES

All the **primordial radionuclides** are metals, with the exception of radon, which is a noble gas. As shown in Table 28.1, most are present at very low

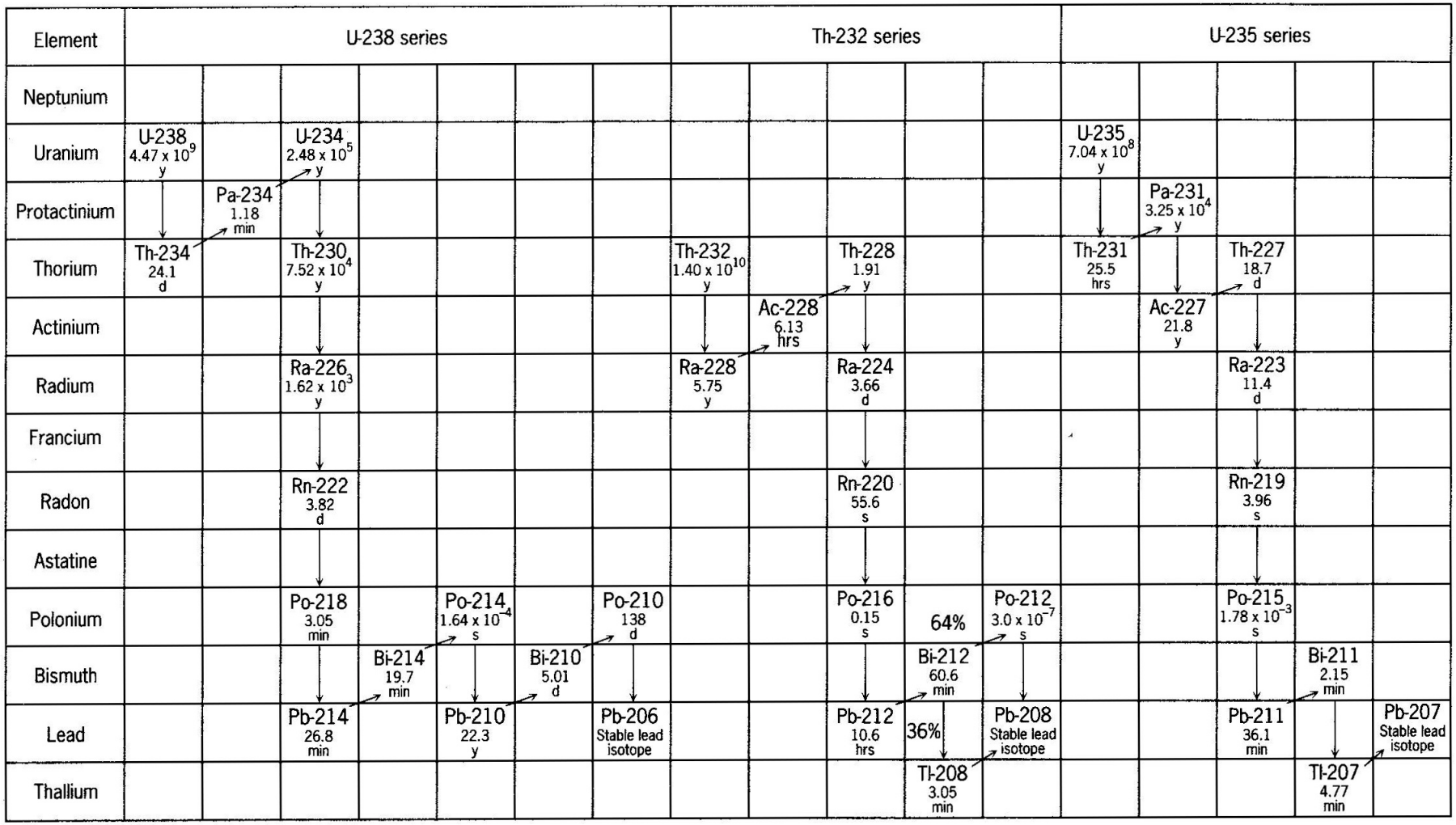

FIGURE 28.3. Chart showing the decay chain of the uranium and thorium series isotopes and the half-lives of each isotope. Alpha decays are shown by the vertical arrows and beta decays by the diagonal arrows. *Source*: From C. Giffin, A. Kaufman, and W. S. Broecker, reprinted with permission from the *Journal of Geophysical Research*, vol. 68, p. 1750, copyright © 1963 by the American Geophysical Union, Washington, DC.

TABLE 28.1
Average Oceanic and Sedimentary Concentrations of the Primordial Radionuclides

Isotope	*Estimated Average Concentration in Seawater (g/L)*	*Estimated Average Concentration in Surface Sediments (g/g)*	*Range of Concentration in Surface Sediments (g/g)*
^{238}U	3.0×10^{-6}	1×10^{-6}	$(0.4–80) \times 10^{-6}$
^{235}U	2.1×10^{-8}	7.1×10^{-9}	
^{234}U	1.6×10^{-10}	8.1×10^{-11}	
^{234}Pa	1.4×10^{-19}	4.7×10^{-20}	
^{231}Pa	$<2 \times 10^{-12}$	1×10^{-11}	$(0.08–9) \times 10^{-11}$
^{234}Th	4.3×10^{-17}	1.4×10^{-17}	
^{232}Th	$<2 \times 10^{-8}$	5.0×10^{-6}	$(1–16) \times 10^{-6}$
^{231}Th	8.6×10^{-20}	2.9×10^{-20}	
^{230}Th	$<3 \times 10^{-13}$	2.0×10^{-10}	$(0.3–20) \times 10^{-10}$
^{228}Th	4.0×10^{-18}	7×10^{-16}	
^{227}Th	$<7.0 \times 10^{-20}$	1.3×10^{-17}	
^{228}Ac	1.5×10^{-21}	2.4×10^{-19}	
^{227}Ac	$<1 \times 10^{-15}$	5.9×10^{-15}	
^{228}Ra	1.4×10^{-17}	2.3×10^{-15}	
^{226}Ra	1.0×10^{-13}	4.0×10^{-12}	$(0.3–40) \times 10^{-12}$
^{224}Ra	2.1×10^{-20}	3.4×10^{-18}	
^{223}Ra	$<4.4 \times 10^{-20}$	8.5×10^{-18}	
^{223}Fr	$<7.0 \times 10^{-24}$	1.4×10^{-21}	
^{222}Rn	6.3×10^{-19}	2.5×10^{-17}	
^{220}Rn	3.3×10^{-24}	5.4×10^{-22}	
^{219}Rn	$<1.7 \times 10^{-25}$	3.1×10^{-23}	
^{218}Po	3.4×10^{-22}	1.4×10^{-20}	
^{216}Po	1.0×10^{-26}	1.7×10^{-24}	
^{215}Po	$<8.1 \times 10^{-29}$	1.4×10^{-26}	
^{214}Po	3.0×10^{-28}	1.1×10^{-27}	
^{212}Po	1.2×10^{-32}	2.4×10^{-29}	
^{211}Po	$<6.8 \times 10^{-29}$	1.2×10^{-26}	
^{210}Po	2.2×10^{-17}	8.8×10^{-16}	
^{214}Bi	2.1×10^{-21}	8.8×10^{-20}	
^{212}Bi	2.2×10^{-22}	3.7×20^{-24}	
^{211}Bi	$<5.6 \times 10^{-24}$	1.0×10^{-21}	
^{210}Bi	7.8×10^{-19}	3.1×10^{-17}	
^{214}Pb	2.9×10^{-21}	1.2×10^{-19}	
^{212}Pb	2.4×10^{-21}	3.9×10^{-19}	
^{211}Pb	$<9.0 \times 10^{-23}$	1.6×10^{-20}	
^{210}Pb	1.1×10^{-15}	4.5×10^{-14}	
^{208}Tl	4.1×10^{-24}	6.7×10^{-22}	
^{207}Tl	$<1.2 \times 10^{-23}$	2.1×20^{-21}	

Source: From *Marine Chemistry*, R. A. Horne, copyright © 1969 by John Wiley & Sons, Inc., New York, p. 295. Reprinted by permission.

concentrations in both seawater and the sediments, making concentration measurements difficult.

The most sensitive technique for quantifying these radionuclides is measurement of their radioactivity. This is commonly done by first chemically separating the isotopes and then measuring the rate at which each produces either α or β^- emissions. This production rate is usually reported as counts per minute and is functionally equal to the decay rate, or **activity** of the radionuclide. Activities are usually reported as **disintegrations per minute (dpm)**. The activity of a radionuclide in a sample of seawater or sediment is reported in terms of dpm/L or dpm/g, respectively. These **specific activities** (A) are directly related to the concentration of the radionuclide as follows:

$$A = \lambda[N] \tag{28.16}$$

The average specific activities of some primordial radionuclides in various water masses are given in Table 28.2.

Secular Equilibrium

For most primordial radionuclides, the half-life of the **daughter** is much shorter than that of the parent. Thus the decay of the **parent** eventually becomes the rate-determining step that controls decay of the daughter, as shown in Figure 28.4. Due to slow decay rates, the concentration of parent and its specific

TABLE 28.2
Average Specific Activities of Some Primordial Radionuclides in Various Water Masses

Isotope	*Daughter Product Half-life (y)*	*Warm Surface Water (dpm/100 kg)*	*North Atlantic Bottom Water (dpm/100 kg)*	*Antarctic Bottom Water (dpm/100 kg)*	*North Pacific Bottom Water (dpm/100 kg)*
^{238}U	Parent	240	240	240	240
^{234}Th	0.066	230	240	240	240
^{234}U	248,000	280	280	280	280
^{230}Th	75,200	<0.02	—	—	0.15
^{226}Ra	1620	7	13	20	34
^{222}Rn	0.010	5	>13	>20	>34
^{210}Pb	22.3	20	8	10	16
^{210}Po	0.38	10	8	10	16
^{235}U	Parent	13	13	13	13
^{231}Pa	32,500	—	—	—	0.05
^{232}Th	Parent	<0.1	<0.1	<0.1	<0.1
^{228}Ra	5.8	3	0.4	—	0.4
^{228}Th	1.9	0.4	0.3	—	0.3

Source: From *Tracers in the Sea*, W. S. Broecker and T. -H. Peng, copyright © 1982 by the Lamont-Doherty Geological Observatory, Palisades, NY, p. 170. Reprinted by permission.

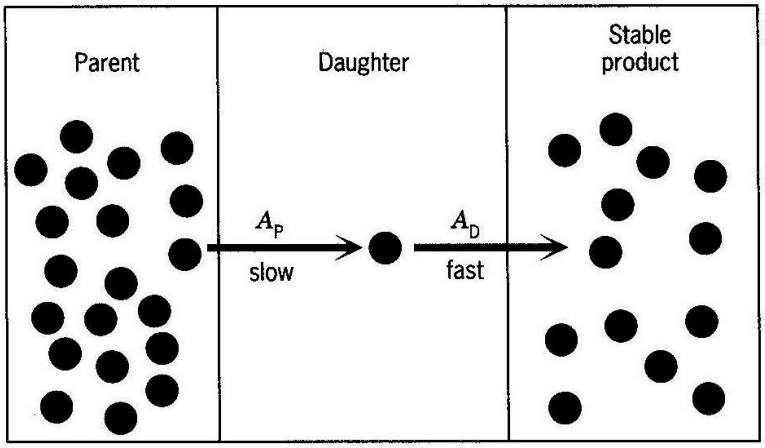

FIGURE 28.4. Secular equilibrium.

activity (A_P) remain relatively constant over time. In the absence of other processes, radioactive decay of these two isotopes will eventually reach a steady state. In this steady state, the rate at which the daughter is supplied from decay of parent (A_P) is matched by its rate of loss via its own decay (A_D). This condition, where $A_P = A_D$, is called **secular equilibrium**.

As shown in Figure 28.5, time is required for the attainment of secular equilibrium. In other words, introduction of the parent radionuclide to seawater

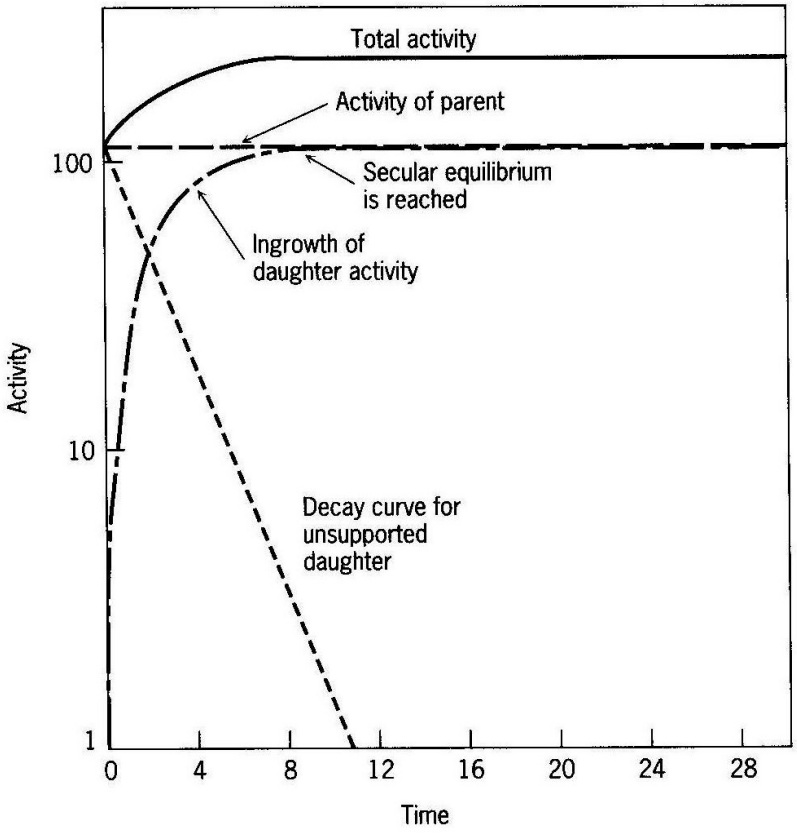

FIGURE 28.5. Secular equilibrium in radioactive decay. *Source*: From *Radioactivity in the Environment*, R. L. Kathren, copyright © 1984 by Harwood Academic Publishers, New York, p. 57. Reprinted by permission.

or sediment will be followed by a period of time during which A_D increases until it reaches a level equal to A_P. The amount of time required to reach secular equilibrium is determined by the half-life of the daughter, as shown in Table 28.3. Thus, given sufficient time and abundance of original parent, all the radionuclides within a decay series should reach secular equilibrium and hence all their specific activities will be equal.

At secular equilibrium, $A_D/A_P = 1$. As shown in Table 28.4, this is not observed for many parent–daughter pairs in the ocean. Most of these ratios

TABLE 28.3
Time Required for Various Daughters of ^{238}U and ^{232}Th To Achieve 99 and 95 Percent of A_P[a]

Nuclide	*99%*	*95%*
^{238}U	Parent	Parent
^{234}Th	160.13 d	104.16 d
^{234}Pa	7.84 min	5.10 min
^{234}U	1.661×10^6 y	1.081×10^6 y
^{230}Th	5.315×10^5 y	3.458×10^5 y
^{226}Ra	1.0777×10^4 y	7.011×10^3 y
^{222}Rn	25.41 d	16.53 d
^{218}Po	20.27 min	13.18 min
^{214}Pb	2.97 h	1.93 h
^{214}Bi	2.18 h	1.42 h
^{214}Po	1.09×10^{-3} s	7.09×10^{-4} s
^{210}Pb	146.18 y	95.09 y
^{210}Bi	33.22 d	21.61 d
^{210}Po	2.51 y	1.63 y
^{206}Pb	Stable (24.1% of natural Pb)	
^{232}Th	Parent	Parent
^{228}Ra	44.52 y	28.96 y
^{228}Ac	40.73 h	26.49 h
^{228}Th	12.62 y	8.21 y
^{224}Ra	24.19 d	15.73 d
^{220}Rn	6.02 min	3.93 min
^{216}Po	1.05 s	0.68 s
^{212}Pb	2.93 d	1.91 d
^{212}Bi	6.7 h	4.36 h
^{212}Po	1.99×10^{-6} s	1.3×10^{-6} s
^{208}Tl	20.6 min	13.4 min
^{208}Pb	Stable (52.3% of natural Pb)	

Source: From *Radioactivity in Geology*, E. M. Durrance, copyright © 1986 by Ellis Horwood, Ltd., Chichester, England, p. 286. Reprinted by permission.

[a]Since secular equilibrium is approached asymptotically, A_P is never quite attained.

TABLE 28.4
Typical Activity Ratios for Daughter–Parent Pairs in Various Water Types

	Estuaries	*Coastal*	*Surface Ocean*	*Deep Sea*
$^{210}Pb/^{226}Ra$	—	—	>1[a]	0.4–1.0
$^{230}Th/^{234}U$	—	—	$<3 \times 10^{-5}$	3×10^{-4}
$^{228}Th/^{228}Ra$	0.01	0.05	0.2	0.5–1.0
$^{234}Th/^{238}U$	0.2	0.6	>0.9	~1
$^{231}Pa/^{235}U$	—	—	—	2×10^{-3}
$^{210}Po/^{210}Pb$	—	—	0.5	1.0

Source: From *Tracers in the Sea*, W. S. Broecker and T.-H. Peng, copyright © 1982 by the Lamont-Doherty Geological Observatory, Palisades, NY, p. 173. Reprinted by permission.
[a]Although ^{210}Pb is being removed from surface water by particles, it has an additional source. Radon atoms escaping to the atmosphere from continental soils decay to ^{210}Pb. These ^{210}Pb atoms are incorporated into aerosols and are brought back to Earth's surface by rain and aerosol impact. The flux of these atoms to the sea surface exceeds by about a factor of 10 the in situ production by radiodecay of ^{226}Ra in the upper 200 m of the ocean.

are less than 1 due to preferential removal of daughter. This is usually the result of some chemical and/or physical process.

The net removal rate of the daughter can be calculated from a steady-state box model, as illustrated in Figure 28.6. The sole source of daughter is assumed to be from decay of the parent. Thus the supply rate of daughter is equal to A_P. At steady state, the supply rate must match the rate at which daughter is lost. The rate at which daughter is lost from its own decay is equal to A_D. Since nothing more is known about the chemical and/or physical processes that affect the daughter, its net nonradioactive removal rate is assumed to be directly proportional to its concentration, $[D]$. Thus

$$\text{Net nonradioactive removal rate} = k_D[D] \tag{28.17}$$

where k_D is the net removal rate constant.

This steady-state model is described by the following mass balance equation in which the supply rate of daughter is on the left and its losses are on the right: that is

$$A_P = A_D + k_D[D] \tag{28.18}$$

Since $A_D = \lambda_D[D]$, $[D]$ can be eliminated from Eq. 28.18 as follows:

$$A_P = A_D + \left[\frac{k_D A_D}{\lambda_D}\right] \tag{28.19}$$

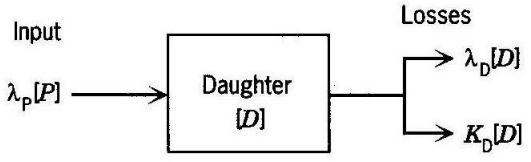

FIGURE 28.6. Steady-state box model for computing net removal rates of radionuclides.

Rearranging and solving for k_D yields

$$k_D = \left[\frac{A_P - A_D}{A_D}\right] \lambda_D \tag{28.20}$$

This equation can be rearranged to

$$k_D = \left[\frac{1 - \dfrac{A_D}{A_P}}{\dfrac{A_D}{A_P}}\right] \lambda_D \tag{28.21}$$

Thus without any knowledge of the actual removal process, its net rate constant can be inferred from A_D/A_P. Note that k_D includes the effects of all nonradioactive processes, whether they be additions or removals of daughter. Thus if daughter is also supplied by some nonradioactive process, its actual removal rate will be somewhat greater than the net removal rate. Further information is required to determine the mechanism by which daughter is removed (or added). But once this is done, the results can be generalized to chemically similar isotopes, such as cogeners or ions with similar charge densities. In this way, radionuclides are used as natural tracers of many marine processes. Several examples are given below.

Determination of Particle Scavenging Rates

The specific activity ratio of $^{228}Th/^{228}Ra$ ($A_{228_{Th}}/A_{228_{Ra}}$) is less than 1 because ^{228}Th is preferentially removed from seawater by adsorption onto sinking particles. The specific activity of ^{228}Ra is maintained by diffusion of this isotope from the sediments. The sediments contain radium because this element is incorporated into the tests of calcareous plankton. Biogenic uptake is favored by the chemical similarity of radium to calcium. ^{228}Ra is also produced from the in situ decay of ^{232}Th.

As shown in Figure 28.7, the effect of particle scavenging on ^{228}Th is most pronounced in coastal waters. This is due to higher particle concentrations and shallower water depths. Under these conditions, ^{228}Th has a greater chance of adsorbing onto particles or the surface sediments. Because of shallow water depths, diffusion of radium from the sediments has a relatively large impact on its specific activity in the water column. Thus relatively high levels of ^{228}Ra also contribute to the occurrence of low $A_{228_{Th}}/A_{228_{Ra}}$'s in coastal waters.

The net rate constant for the removal of ^{228}Th can be calculated by substituting the observed specific activity ratios into Eq. 28.21. This information is commonly reported as a scavenging turnover time in years ($1/k_D$). Indeed, this is how the scavenging turnover times were obtained for some of the trace metals listed in Table 11.3. This rate information is also commonly given as the chemical half-life, or half-scavenging time, of an isotope ($0.693/k_D$). This can be thought of as the time it would take for the nonradioactive processes to remove half of the isotope's specific activity. As shown in Figure 28.8, the

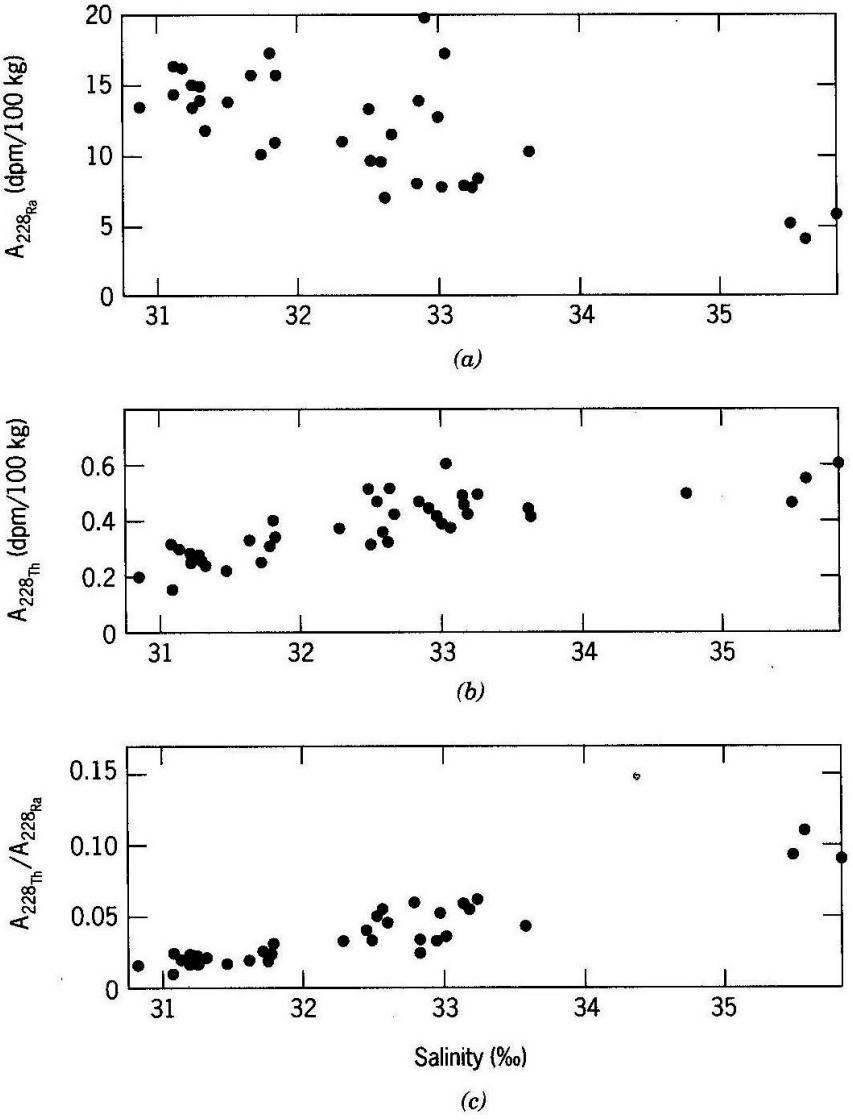

FIGURE 28.7. Specific activities of (*a*) ^{228}Ra, (*b*) ^{228}Th, and (*c*) ^{228}Th/^{228}Ra as a function of salinity in coastal samples taken adjacent to New York City. Due to the input of river water, the waters closest to the coast have the lowest salinity. Thus the increase in salinity is a measure of distance from the shore. *Source*: From Y.-H. Li, H. W. Feely, and P. H. Santschi, reprinted with permission from *Earth and Planetary Science Letters*, vol. 42, p. 20, copyright © 1979, Elsevier Science Publishers, Amsterdam, The Netherlands.

half-scavenging time for ^{228}Th ranges from approximately 0.1 to 1.0 y in the surface waters of the open ocean.

In the open ocean, $A_{228_{Th}}/A_{228_{Ra}}$ increases with depth through the mixed layer and sometimes exceeds 1 at its base. This excess ^{228}Th is thought to be supplied by the remineralization of biogenic particles. In other words, marine organisms appear to bioaccumulate ^{228}Th.

The radioactive half-life of ^{234}Th is only 24 d. Thus its use as a tracer of scavenging is limited to coastal waters where high particle concentrations ensure rapid removal rates. At these locations, ^{234}Th distributions yield half-

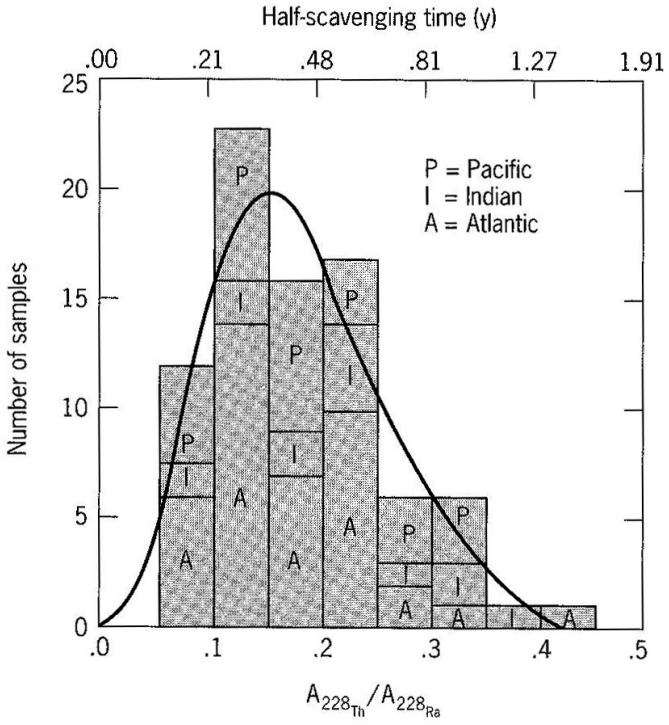

FIGURE 28.8. The specific activity ratio of $^{228}Th/^{228}Ra$ and the half-scavenging time for ^{228}Th in the open ocean surface waters of the Atlantic, Pacific, and Indian oceans. *Source*: From W. S. Broecker, A. Kaufman, and R. M. Trier, reprinted with permission from *Earth and Planetary Science Letters*, vol. 20, p. 41, copyright © 1973, Elsevier Science Publishers, Amsterdam, The Netherlands.

scavenging times similar to that of ^{228}Th. Because of its relatively short half-life, ^{234}Th cannot be used to measure scavenging rates in open ocean waters. In these waters, particle concentrations are so low that the ^{234}Th would decay before it had a chance to adsorb. As a result, $A_{234_{Th}}/A_{238_U}$ in open ocean waters is close to 1. This illustrates an important factor that must be considered when selecting an isotope as a tracer for a particular geochemical process; its decay rate must be close to the rate of the process to be studied. As shown in Table 28.5, mismatches produce activity ratios too close to 1 or too small to be precisely measured.

In Case 1, $k_D >>> \lambda_D$, so the chemical half-life is much shorter than the radioactive half-life. Rapid removal keeps A_D very low and hence results in a very small specific activity ratio that is difficult to measure precisely. In Case

TABLE 28.5
Comparison of the Combined Effects of Chemical and Radioactive Removal on the Specific Activity Ratios of a Parent–Daughter Radionuclide Pair[a]

Case	k_D (y^{-1})	*Chemical* $t_{\frac{1}{2}}$ (y)	λ_D (y^{-1})	*Radioactive* $t_{\frac{1}{2}}$ (y)	*Calculated* A_D/A_P
1	0.69	1.0	0.0069	100	0.0099
2	0.0069	100	0.0069	100	0.50
3	0.0069	100	0.69	1.0	0.99

[a] A_D/A_P is inferred from the given net removal rate constants and radioactive half-lives using Eq. 28.21.

3, $k_D <<< \lambda_D$, so the chemical half-life is much longer than the radioactive half-life. Removal is too slow to cause secular disequilibrium and hence the specific activity ratio is close to, and difficult to precisely distinguish from, 1. In Case 2, $k_D = \lambda_D$, so the chemical and radioactive half-lives are equal. Here removal is fast enough to cause secular disequilibrium, but not so fast as to lower A_D greatly. In this situation, when A_D is significantly different from A_P, but not too different, k_D can be calculated with the greatest analytical precision.

Thus ^{230}Th, with a half-life of 75,000 y, is more suitable than ^{234}Th ($t_{\frac{1}{2}}$ = 24 d) or ^{228}Th ($t_{\frac{1}{2}}$ = 1.91 y) for determining half-scavenging times in the deep sea. As shown in Figure 28.9, the half-scavenging times of this isotope decrease with depth in the open ocean probably due to decreasing particle concentrations. Such data also indicate that the adsorption of ^{230}Th on sinking particles must be reversible.

The fate of pollutant lead in the ocean has also been investigated by inferring its scavenging rate from specific activity data. The burning of leaded gasoline injects lead aerosols into the atmosphere, some of which settle onto the sea surface. This aeolian input causes the surface-water lead enrichment ($A_D/A_P > 1$) shown in Figure 28.10. ^{210}Pb is also supplied to the ocean via decay of its parent, ^{226}Ra. The specific activity of ^{226}Ra increases with depth, because most is supplied by diffusion from the sediments. As mentioned above, radium is resolubilized in the sediments from biogenic calcium carbonate. ^{226}Ra is also produced from the decay of ^{230}Th transported to the sediments via particle scavenging.

At mid depths, A_{210Pb}/A_{226Ra} is less than 1, suggesting that lead is removed faster than radium, probably by adsorption onto sinking particles. With these activity values, the chemical half-life of lead in the midwaters is calculated to be 100 y. Near the seafloor, the chemical half-life of lead is shorter (15 y) due

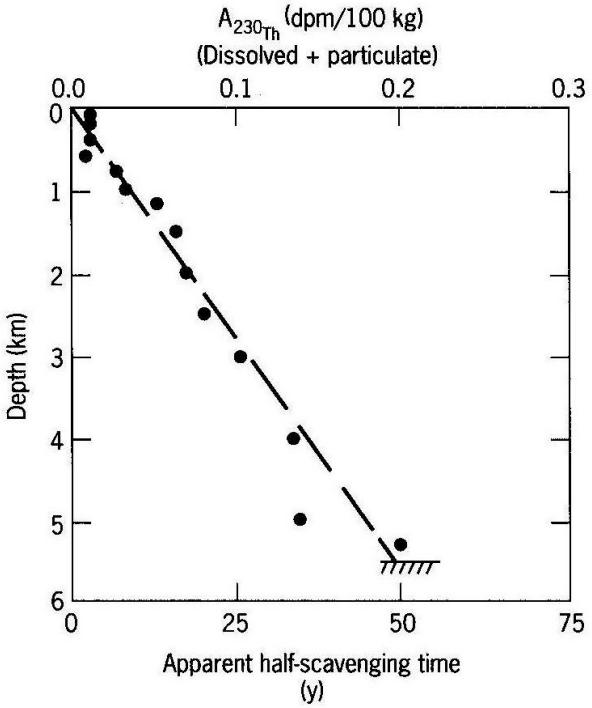

FIGURE 28.9. The specific activity of ^{230}Th and its apparent half-scavenging time as a function of depth at a site in the northwest Pacific. The specific activity of the parent, ^{234}U, at this site is 280 dpm/100 kg. The dissolved A_{230th} is ten times greater than the particulate activity. *Source*: From Y. Nozaki, Y. Horibe, and H. Tsubota, reprinted with permission from *Earth and Planetary Science Letters*, vol. 54, p. 213, copyright © 1981, Elsevier Science Publishers, Amsterdam, The Netherlands.

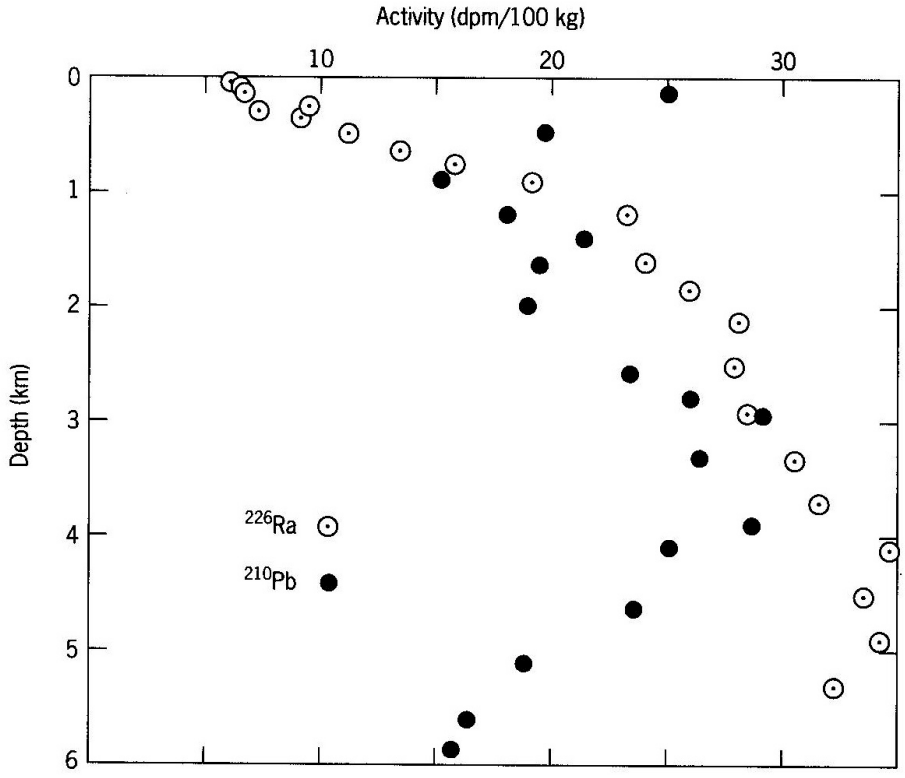

FIGURE 28.10. Specific activities of ^{226}Ra and ^{210}Pb versus depth at GEOSECS Station 214 (32°N 177°W) in the central north Pacific. *Source*: From *Tracers in the Sea*, W. S. Broecker and T.-H. Peng, copyright © 1982 by the Lamont-Doherty Geological Observatory, Palisades, NY, p. 193. Reprinted by permission. ^{226}Ra data from Y.-C. Chung and H. Craig, reprinted with permission from *Earth and Planetary Science Letters*, vol. 49, p. 271, copyright © 1980, Elsevier Science Publishers, Amsterdam, The Netherlands. ^{210}Pb data from Y. Nozaki, K. K. Turekian, and K. von Damm, reprinted with permission from *Earth and Planetary Science Letters*, vol. 49, p. 395, copyright © 1980, Elsevier Science Publishers, Amsterdam, The Netherlands.

to adsorption onto the surface sediments. Using estimates of anthropogenic lead input, the chemical half-life in the surface waters has been estimated to be less than 20 y. ^{210}Pb decays to ^{210}Po. Polonium is much more reactive than lead and has a very high enrichment factor in the tissues of marine organisms. As a result, its chemical half-life in surface waters is only about 0.4 y.

Dating Marine Sediments and Determining Sedimentation Rates

As indicated above, some daughters of the primordial radionuclides are preferentially transported to the seafloor via particle scavenging and/or by incorporation into biogenic particles. Since the rain rate of daughter exceeds that of its parent, the surface sediments have $A_D/A_P > 1$.

Once in the sediment, the parent will undergo decay and thus contribute to the A_D in the sediments. This contribution is termed the supported A_D. As

noted above, preferential particle scavenging of the daughter causes the total A_D in the surface sediments to be somewhat larger than the supported A_D. This excess activity is termed the unsupported A_D and is equal to $A_D - A_P$. A_P is nearly constant with depth due to slow rates of radioactive decay. Hence the supported A_D is nearly constant with depth. In contrast, the sediment is cut off from its source of unsupported A_D following burial. Thus the unsupported A_D decreases with depth, as shown in Figure 28.11.

The time that has elapsed since particles, now at depth z, were last at the sediment surface can be calculated from the decrease in unsupported (or excess) A_D with depth. To do this, it must be assumed that the sedimentation rate (s) and the supply of unsupported A_D to the sediments has not varied over time. Since $s = z/t$, the radioactive decay law (Eq. 28.13) can be written as

$$\frac{A_{\mathrm{DExcess}_z}}{A_{\mathrm{DExcess}_{z=0\,\mathrm{cm}}}} = e^{-\lambda_D \frac{z}{s}} \tag{28.22}$$

where the radionuclide concentration, $[N]$, is given in terms of its specific

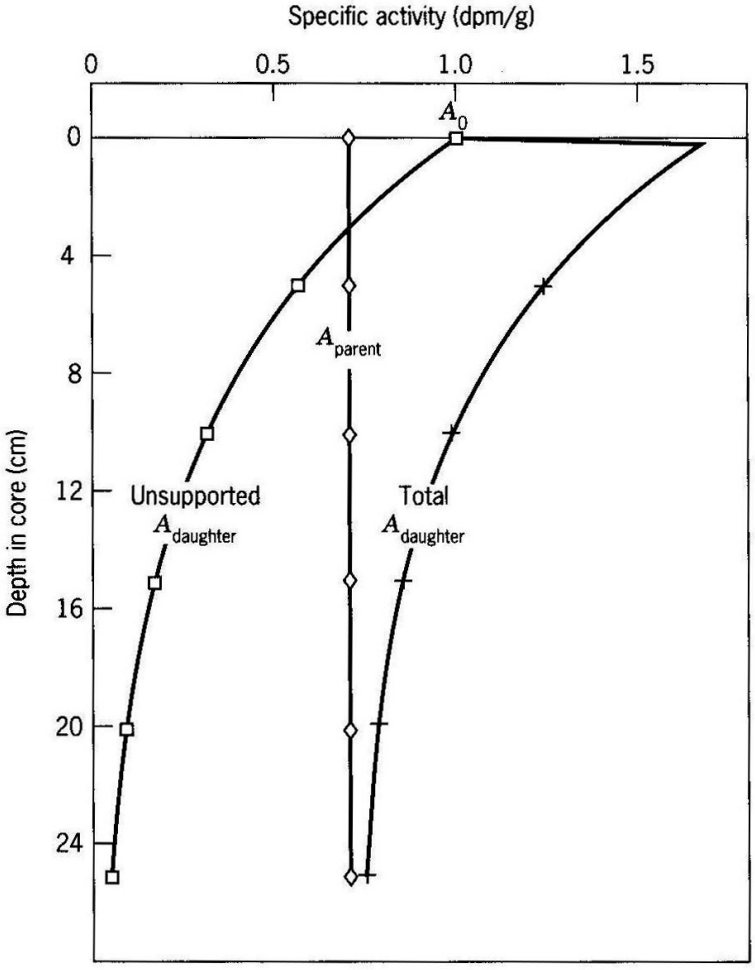

FIGURE 28.11. A_P, supported and unsupported A_D of a parent–daughter radionuclide pair in sediment core. The half-life of the daughter is 5700 y and the sedimentation rate is 1 cm/1000 y. Note that some time is required for the supported A_D to reach secular equilibrium with A_P. This causes A_D to increase with depth in the top few

activity, A_D (i.e., dpm/g). This can be rearranged to yield the equation of a straight line: that is,

$$\ln A_{\mathrm{DExcess}_z} = -\frac{\lambda_D}{s} z + \ln A_{\mathrm{DExcess}_{z=0\,\mathrm{cm}}} \tag{28.23}$$

in which the slope is inversely proportional to the sedimentation rate. This is illustrated for an idealized data set in Figure 28.12*b*.

As shown in Figure 28.13, radionuclide distributions in sediments are noisy. Thus sedimentation rates must be inferred from "best-fit" equations determined by the method of linear regression. Alternatively, sedimentation rates are reported as the range of values that bracket the data. Some of this noise is the result of bioturbation. Some is also caused by variations in sedimentation rate and in the supply rate of daughter. Thus it is best to corroborate these inferred sedimentation rates using other radionuclide pairs that undergo decay and chemical transport over somewhat different time scales and by different mechanisms. For example, accretion rates of iron–manganese nodules have been inferred from several primordial radionuclide pairs. These radionuclides are incorporated into the nodules during the accretion process. As shown in Figure 28.14*a*, the ^{238}U–^{230}Th and ^{235}U–^{231}Pa pairs yield accretion rates of 4.0 and 4.3 mm per million years, respectively. This is close to that obtained from the ^{238}U–^{234}U pair (Figure 28.14*b*).

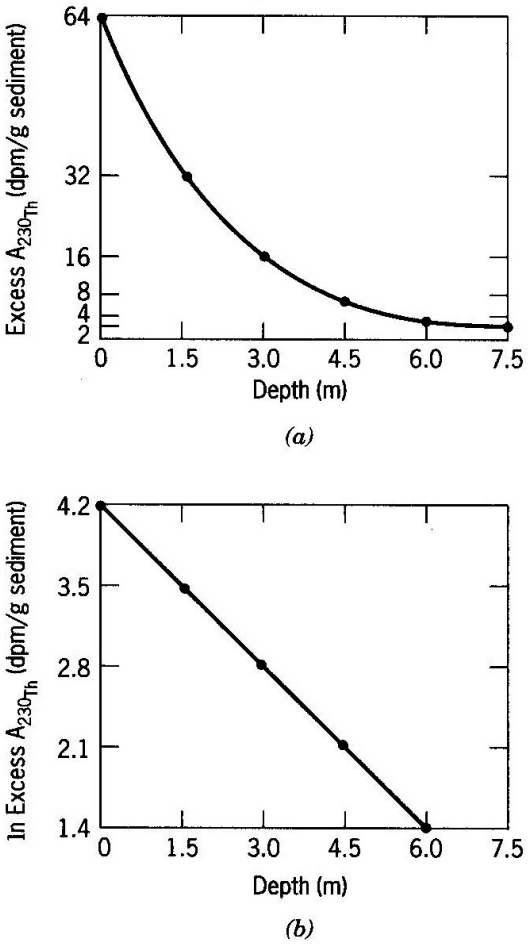

FIGURE 28.12. (*a*) Excess $A_{230_{Th}}$ and (*b*) log Excess $A_{230_{Th}}$ versus depth. This is for an ideal core in which the rate of ^{230}Th input has been constant over time and the sedimentation rate has also been constant at 2.0 cm/1000 y. *Source*: From *Chemical Oceanography*, W. S. Broecker, copyright © 1974 by Harcourt, Brace, and Javanovich Publishers, Orlando, FL, p. 78. Reprinted by permission.

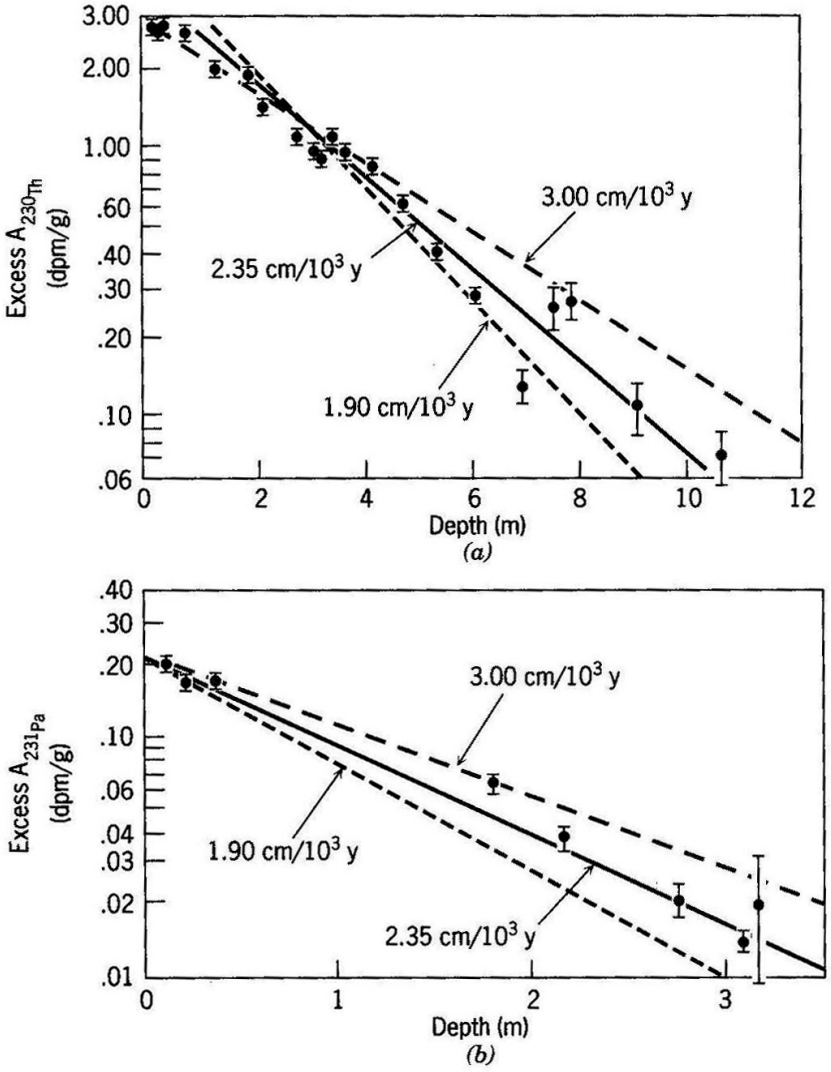

FIGURE 28.13. Actual excess specific activities of (*a*) ^{230}Th and (*b*) ^{231}Pa measured in a sediment core from the Caribbean Sea. The solid line is the best fit as determined by the method of linear regression. *Source*: From W. S. Broecker and J. van Donk, reprinted with permission from *Reviews of Geophysics and Space Physics*, vol. 8, p. 176, copyright © 1970 by the American Geophysical Union, Washington, DC.

Because the accretion rates are very slow, the activities of ^{231}Pa and ^{230}Th have been lowered to their detection limits within 1 mm of the nodule's surface. The half-life of ^{234}U is an order of magnitude longer; thus it can be detected 4 mm into the nodule. The time limits of application for other commonly used radionuclides are given in Figure 28.15. The datable time spans will expand as improvements in analytical technology lower detection limits.

Though not part of an extended decay series, ^{40}K is another primordial radionuclide. This isotope is ubiquitous in igneous rocks and decays to either ^{40}Ca or ^{40}Ar. Since the latter is a gas, it is not present in the rock at the time of solidification. Any ^{40}Ar now present in an igneous rock has been produced by in situ decay and can be used to determine the time that has elapsed since solidification. Due to the long half-life of ^{40}K (approximately 1 billion years),

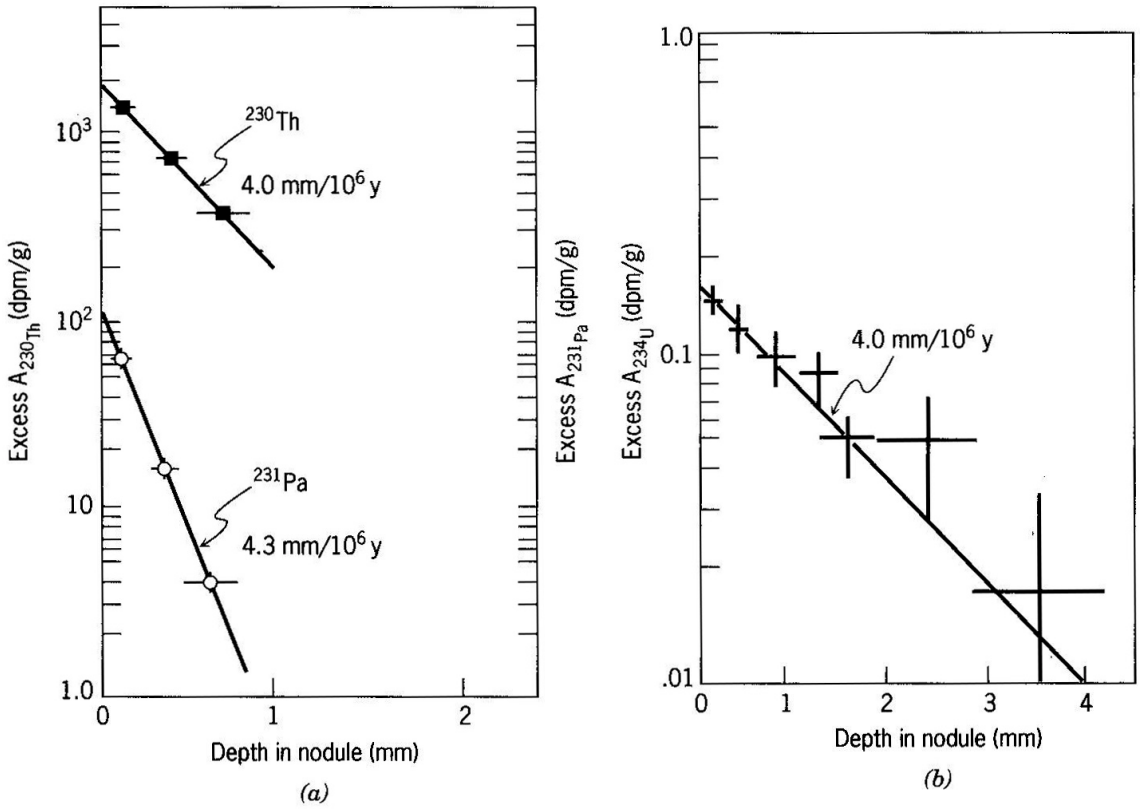

FIGURE 28.14. (*a*) Log Excess ^{230}Th and ^{231}Pa specific activities versus depth in a manganese nodule from the north Pacific Ocean. The computed accretion rates are given in mm per million years. (*b*) Log excess ^{234}U versus depth in the same manganese nodule. The line predicted from the ^{230}Th results is shown for reference. *Source*: From T. L. Ku and W. S. Broecker, reprinted with permission from *Earth and Planetary Science Letters*, vol. 2, pp. 319–320, copyright © 1967, Elsevier Science Publishers, Amsterdam, The Netherlands.

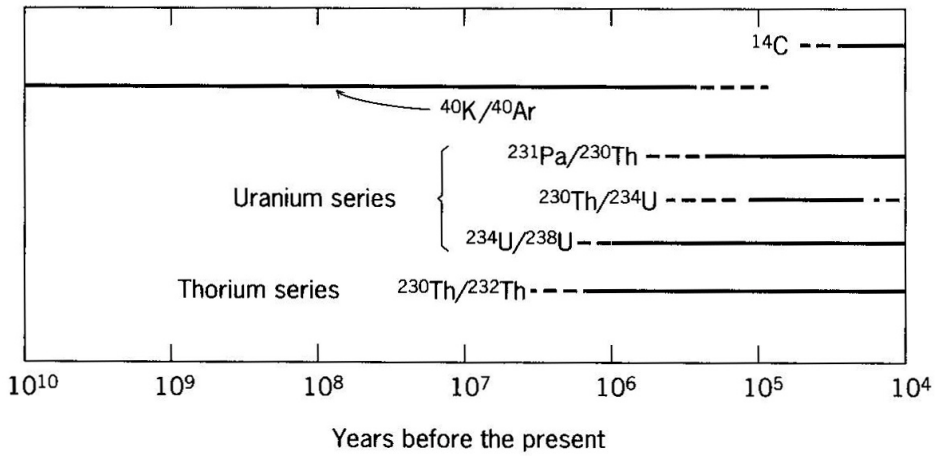

FIGURE 28.15. Time limitations on the application of radionuclides for determination of absolute ages of sediment deposits and times of rock formation. *Source*: From *Oceanography: A View of the Earth*, 4th ed., M. G. Gross, copyright © 1987 by Prentice Hall, Inc., Englewood Cliffs, NJ. Reprinted by permission.

400,000 y must pass before ^{40}Ar reaches measurable levels. Thus, the ^{40}K–^{40}Ar couple can date only those rocks older than 400,000 y.

Despite this limitation, the ^{40}K–^{40}Ar couple has been widely used as a dating tool. For example, it has been used to determine Earth's age and to date magnetic field reversals. The timing of magnetic field reversals has been used to support the theory of plate tectonics and to infer rates of seafloor spreading. ^{40}K–^{40}Ar has also been used to date volcanic ash layers, such as those at the Cretaceous–Tertiary boundary. Caution must be used in this application, as the date recorded by the isotopes is the time since the particles solidified. Due to resuspension and transport by bottom currents, ash layers can be composed of igneous material deposited at a time much later than its solidification. In such cases, potassium–argon dates will be too old. Spuriously young ages can be produced if the rocks have been subjected to elevated temperatures and pressures as this causes partial loss of argon.

Determination of Diffusion Rates and Diffusivity Constants

The primordial radionuclides and radiocarbon have been used to determine diffusion rates as well as the values of diffusivity coefficients. Two examples are given here. The first demonstrates how ^{222}Rn and ^{226}Ra have been used to study gas exchange at the air–sea interface. The second shows how rates of vertical diffusion in the deep sea have been measured from ^{228}Ra and ^{222}Rn.

As shown in Figure 28.16, the diffusion of ^{222}Rn across the air–sea interface causes its specific activity to be lower than that predicted from secular equilibrium with its parent, ^{226}Ra. This net flux of radon from the ocean to the atmosphere indicates that the surface waters are supersaturated with respect to this gas. The difference in specific activity between the parent and daughter ($A_{226Ra} - A_{222Rn}$) is a measure of how much ^{222}Rn has been degassed from the mixed layer.

The thermocline acts as a barrier that inhibits mixing between the deep and surface waters. Thus deep-water ^{222}Rn decays before it can diffuse through the density barrier into the mixed layer. This is why the depth of the mixed layer coincides with the lower boundary of the ^{222}Rn-deficient waters. Assuming that ^{222}Rn is present in a steady state in which its only supply to the mixed layer is via in situ decay of ^{226}Ra and its only losses are from decay and gas exchange, the following mass balance equation can be constructed:

$$hA_{226Ra} = hA_{222Rn} + F \tag{28.24}$$

In this equation, h is the depth of the mixed layer and the activities are average values representative of the mixed layer. Solving for F, the gas flux, yields

$$F = h(A_{226Ra} - A_{222Rn}) \tag{28.25}$$

This flux can also be inferred from the stagnant-film model as presented

For the conditions illustrated in Figure 28.16, $z = 28$ μm. Results from other sites range from 0 to 120 μm and are similar to those obtained from CO_2 fluxes as measured by the gas' ^{14}C content. These results are currently being used to predict global ocean fluxes of anthropogenic gases such as CO_2.

Both ^{226}Ra and ^{228}Ra are produced in the sediments via decay from thorium parents. Both are also remobilized from the sediments as a result of the remineralization of biogenic calcium carbonate. Some of this radium diffuses into the deep ocean and some decays. The ^{222}Rn produced from decay of ^{226}Ra also diffuses into the bottom waters. Since ^{222}Rn is transported faster than ^{226}Ra, it is present in excess in the deep waters. As shown in Figure 28.17, this unsupported ^{222}Rn decreases with increasing height above the seafloor. A similar situation is observed for ^{228}Ra, whose parent is the insoluble ^{232}Th. ^{228}Ra penetrates higher into the deep waters due to its longer half-life and thus can be used to study mixing processes over a much larger depth range than ^{222}Rn.

On short time scales, vertical diffusion is the most important process transporting these isotopes. Thus their vertical distributions can be used to infer vertical "diffusion" rates, as well as the value of the vertical diffusivity coefficient, D_z. In this application, "diffusion" represents the combined effects

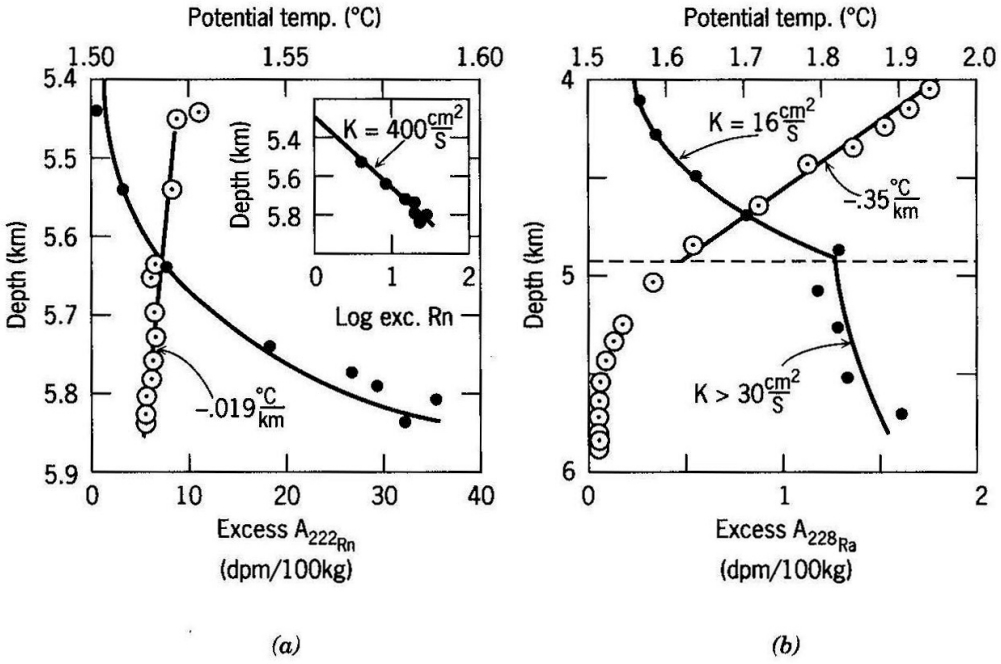

FIGURE 28.17. (*a*) Excess $A_{222_{Rn}}$ and (*b*) Excess $A_{228_{Ra}}$ versus depth in the deep water at 24°N 54°W in the north Atlantic. Also included are the potential temperature gradients. *Source*: From *Tracers in the Sea*, W. S. Broecker and T.-H. Peng, copyright © 1982 by the Lamont-Doherty Geological Observatory, Palisades, NY, p. 585. Reprinted by permission. After J. L. Sarmiento, H. W. Feely, W. S. Moore, A. E. Bainbridge, and W. S. Broecker, reprinted with permission from *Earth and Planetary Science Letters*, vol. 32, p. 362, copyright © 1976, Elsevier Science Publishers, Amsterdam, The Netherlands.

of eddy and molecular diffusion, where the former is likely to be much larger than the latter. If this diffusive mixing and radioactive decay are the sole processes affecting the radionuclides, their vertical distributions can be described by the following equation:

$$A_z = A_o e^{-\sqrt{\frac{\lambda}{D_z}}z} \tag{28.28}$$

In this equation, A_o and A_z are the excess A_D's present at the sediment surface and at some depth z above the seafloor, respectively.

Thus A_z should decrease exponentially with increasing depth above the seafloor. This behavior is verified by the linear relationship observed between log A_z and depth as shown in the insert in Figure 28.17*a*. The depth ($z_{\frac{1}{2}}$) at which A_z has declined to one-half its original value ($A_o/2$) is equal to $0.693\sqrt{D_z/\lambda}$. Thus $D_z = \lambda(z_{\frac{1}{2}}/0.693)^2$.

At this site in the North Atlantic, the $z_{\frac{1}{2}}$'s are such that the deep-water ^{222}Rn and ^{228}Ra distributions yield D_z's of 400 and 16 cm^2/s. These values lie within the range given in Figure 4.13 for oceanic eddy diffusion coefficients. The substantial dissimilarity in these estimates is probably due to differences in their chemical behavior and rates of radioactive decay. Since ^{228}Ra has a longer half-life, its distribution reflects the effects of mixing over longer time and space scales. In other words, the vertical distribution of ^{222}Rn is more influenced by short-term fluctuations in environmental conditions and water motion. The fairly large difference in these estimates of D_z suggests that mixing over long time and space scales is functionally distinct from that which occurs over short time and space scales.

As shown in Figure 28.17*b*, an abrupt change in the temperature gradient is present at 5 km, suggesting the presence of another water mass. The D_z in the overlying water mass is somewhat less than that in the lower one. This suggests that the rate of vertical diffusion is inversely related to the density gradient. In other words, the steeper the gradient, the slower the rate of vertical diffusion.

Though the half-life of ^{228}Ra is longer than that of ^{222}Rn, it is still too short (6 y) to use as a tracer of diffusive mixing on the time and space scales over which thermohaline circulation occurs. Since the half-life of ^{226}Ra is much longer (1600 y), marine chemists had hoped that this isotope could be used to measure some aspects of global oceanic circulation. As with ^{228}Ra, this isotope diffuses from the sediments, but its release is geographically variable. Until this variability is quantified, ^{228}Ra cannot be used as a tracer of large-scale oceanic circulation.

COSMOGENIC RADIONUCLIDES

Cosmic rays are charged particles that enter Earth's atmosphere from outer space. They are mostly protons (87%) and α particles (12%), though some larger nuclei (1%) are present. Their energies range up to 10^{14} MeV. Atmospheric

gases are ionized as a result of collision with the low-energy cosmic rays. The high-energy cosmic rays can cause fragmentation of the gas nuclei. High-energy neutrons are also given off as a result of these **spallation reactions**. The energy of these neutrons is lowered by repeated collisions with gas atoms. When their energy has been sufficiently lowered, these neutrons can be captured by the nucleus of a gas atom. As shown in Figure 28.18, the capture of a neutron by an atom of $^{14}_{7}N$ is accompanied by the ejection of a proton, resulting in the formation of $^{14}_{6}C$.

As described below, oceanic **radiocarbon** measurements have been used to measure rates of water motion, sedimentation, bioturbation, and the timing of sea level changes. Other **cosmogenic radionuclides** that have provided information about marine processes include ^{3}H, ^{7}Be, ^{10}Be, ^{26}Al, and ^{32}Si. Their half-lives and global distributions are given in Table 28.6.

^{10}Be dissolves in rainwater and is adsorbed onto atmospheric particles. Following atmospheric fallout as rain or aerosols, ^{10}Be is transported to the seafloor by particle scavenging. Since this flux is relatively large, ^{10}Be can be used to measure sedimentation rates if its rain rate, as well as that of the other particles, has remained constant over time. Thus the atmospheric production rate of ^{10}Be must also have been constant. Changes in the flux of cosmic rays have caused variations in the ^{10}Be production rate and thus must be corrected for. Alternatively, these natural variations can be used as a record of changes in the cosmic ray flux if the sedimentation rate is independently known.

In addition to deposition in the sediment, some ^{10}Be is incorporated into manganese nodules. Due to its relatively long half-life (1.5×10^6 y), ^{10}Be can be detected far deeper into the nodules than the primordial radionuclides. As shown in Figure 28.19, the accretion rates inferred from the ^{10}Be data range from 2.4 to 4.5 mm per million years, confirming the primordial radionuclide results.

Cosmogenic ^{14}C is incorporated into carbon dioxide gas and transferred from the atmosphere to the ocean via gas exchange across the air–sea interface.

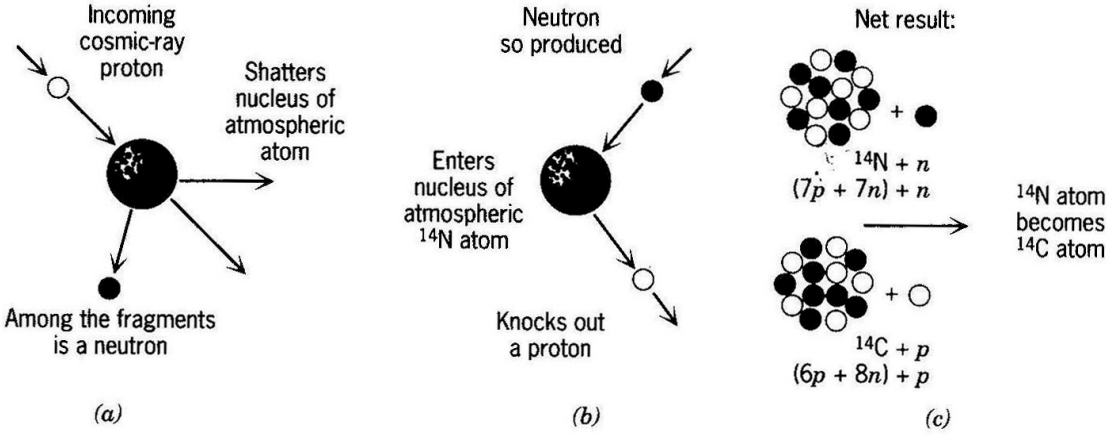

FIGURE 28.18. Production of $^{14}_{6}C$ by spallation. *Source*: From *Tracers in the Sea*, W. S. Broecker and T.-H. Peng, copyright © 1982 by the Lamont-Doherty Geological Observatory, Palisades, NY, p. 238. Reprinted by permission.

TABLE 28.6
Basic Information Concerning Nuclides Produced by Cosmic Rays

	Nuclide					
	^{3}H	^{7}Be	^{10}Be	^{14}C	^{26}Al	^{32}Si
Half-life (y)	12.3	0.145	2.5×10^{6}	5680	7.4×10^{5}	500
Production rate in total atmosphere (atom cm^{-2} s^{-1})	0.25	0.081	0.045	2.5	1.4×10^{-4}	1.6×10^{-4}
Fraction of total earth inventory in						
Atmosphere	0.072	0.71	3.9×10^{-7}	0.019	1.4×10^{-6}	2.0×10^{-3}
Land surface	0.27	0.08	0.29	0.04	0.29	0.29
Ocean—mixed layer	0.35	0.2	5.7×10^{-6}	0.022	1.4×10^{-5}	0.0035
Ocean–excluding mixed layer	0.3	0.002	10^{-4}	0.92	7×10^{-5}	0.68
Oceanic sediments	0	0	0.71	0.004	0.71	0.028
Average concentration in ocean (10^{-3} dpm kg $water^{-1}$)	36	—	10^{-3}	260	1.2×10^{-5}	2.4×10^{-2}
Average specific activity in ocean (dpm g $element^{-1}$)	3.3×10^{-4}	—	1600	10	0.0012	0.008
Global inventory (kg)	3.5	3.2×10^{-3}	4.3×10^{5}	7.5×10^{4}	1.1×10^{3}	1.4
Global inventory (MCi)	35	1.1	6.4	340	0.020	0.023

Source: From *Chemical Oceanography*, vol. 3, J. D. Burton (eds: J. P. Riley and G. Skirrow), copyright © 1975 by Academic Press, Orlando, FL, p. 140. Reprinted by permission. Data from *The Handbook of Physics, 2E*, E. U. Condon and H. Odishaw, copyright © 1967 by McGraw–Hill, Inc., New York, pp. 9.277, 9.285, 9.319. Reprinted by permission.

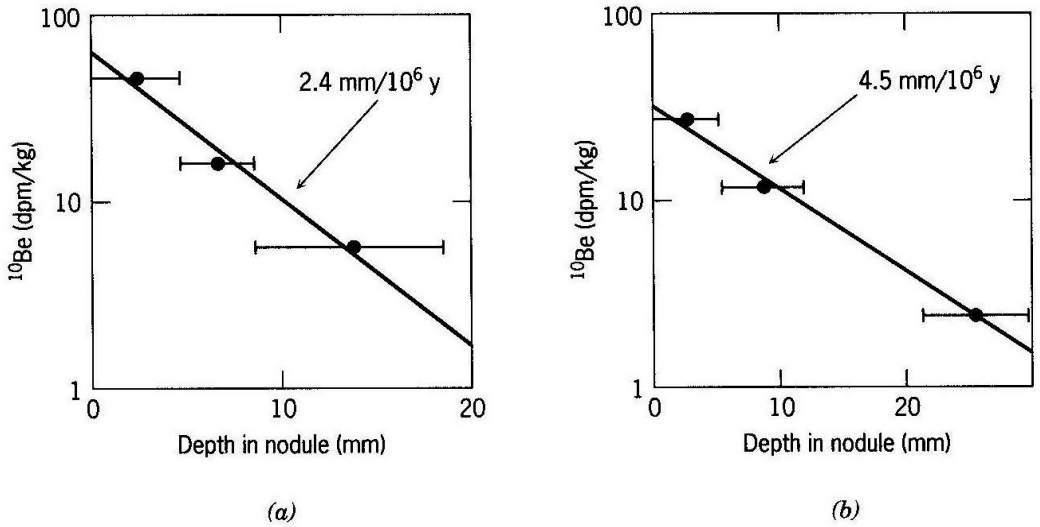

FIGURE 28.19. Log $A_{^{10}Be}$ as a function of depth in a manganese nodule from the (*a*) north Pacific Ocean (20°N 174°E) and (*b*) south Atlantic Ocean (28°S 41°W). *Source*: From *Tracers in the Sea*, W. S. Broecker and T.-H. Peng, copyright © 1982 by the Lamont-Doherty Geological Observatory, Palisades, NY, p. 265. Reprinted by permission. Data from (*a*) *Marine Geology and Oceanography of the Pacific Manganese Nodule Province*, T. L. Ku, A. Omura, and P. S. Chen (eds.: J. L. Bischoff and D. Z. Piper), copyright © 1979 by Plenum Press, New York, p. 801 (reprinted by permission); (*b*) K. K. Turekian, J. K. Cochran, S. Krishnaswami, W. A. Sanford, P. D. Parker, and K. A. Bauer, reprinted with permission from *Geophysical Research Letters*, vol. 6, p. 419, copyright © 1979 by the American Geophysical Union, Washington, DC.

Due to its relatively fast decay rate, radiocarbon is not homogeneously distributed through the ocean and exhibits significant vertical and horizontal segregation. In general, the oldest waters have the lowest radiocarbon content. Therefore radiocarbon tends to decrease with depth. In the deep waters, radiocarbon tends to decrease with increasing distance from the site of water mass formation. Due to continual input of "young" carbon via the remineralization of sinking biogenic particles, radiocarbon measurements cannot be directly converted into water-mass ages.

Radiocarbon gradients can be used to measure rates of ocean mixing. As illustrated below, oceanic radiocarbon distributions have been used to compute the rate of vertical mixing, v_{mix}, between the surface and deep reservoirs. This rate is used in the Broecker box model of vertical segregation.

In the lab, ^{14}C is commonly measured in terms of its abundance relative to the total carbon in a sample, (i.e., as $^{14}C/C$), which is hereafter represented as R. Thus the flux of radiocarbon into the deep reservoir of the Broecker box model is given by the sum of its transport via downwelling ($v_{mix}C_{surface}R_{surface}$) and by remineralization of sinking particulate carbon. ($C_{surface}$ is the total concentration of dissolved carbon [ΣCO_2] in the surface water.) Most particulate carbon is deposited by surface-dwelling organisms and thus has a ^{14}C content equal to that of surface-water DIC ($R_{surface}$). If the flux of remineralizable

particulate carbon is represented by B, then the input of ^{14}C to the deep waters as a result of particle transport is given by BR_{deep}.

Assuming that the radiocarbon is in steady state, its inputs to the deep reservoir must equal its losses via upwelling ($v_{mix}C_{deep}R_{deep}$) and radioactive decay ($V_{deep}C_{deep}R_{deep}\,\lambda$) where V_{deep} represents the volume of the deep zone. Thus the following mass balance equation can be written for the deep reservoir:

$$v_{mix}C_{surface}R_{surface} + BR_{deep} = v_{mix}C_{deep}R_{deep} + V_{deep}C_{deep}R_{deep}\,\lambda \quad (28.29)$$

B can be eliminated from this equation using algebraic reasoning similar to that employed in Chapter 9 to replace P, the biogenic particle flux. The resulting equation can be rewritten as

$$v_{mix} = \frac{\lambda V_{deep}}{\frac{R_{surface}}{R_{deep}} - 1} \quad (28.30)$$

The volume of the deep water is equal to hA_{ocean}, where h is the average thickness of the deep reservoir (3 km) and A_{ocean} is the average surface area of the deep reservoir. Thus Eq. 28.30 can be written as:

$$v_{mix} = \frac{\lambda h A_{ocean}}{\frac{R_{surface}}{R_{deep}} - 1} \quad (28.31)$$

Since the average $R_{surface}/R_{deep}$ is 1.12, v_{mix}/A_{ocean} is equal to 300 cm/y. In other words, the annual amount of water exchanged between the surface and deep reservoirs is equal to the volume of water contained in a hypothetical layer that covers the entire ocean surface and is 300 cm thick. Since the deep reservoir has an average thickness of 3000 m, the residence time of water in this zone is given by

$$\text{Residence time of deep water} = \frac{3000\text{ m}}{300\text{ cm/y}} = 1000\text{ y} \quad (28.32)$$

In reality, these reservoirs are not homogeneous. More sophisticated models of elemental cycling take this into account by partitioning the ocean into many more reservoirs. This approach is now being used to predict the rate at which anthropogenic CO_2 is being transported into and through the ocean.

This use of the Broecker box model also assumes that the amount of radiocarbon, and hence the $^{14}C/C$, in the ocean has remained constant over time. While this might have been true in the past, the "natural" ratio has been greatly altered as a result of two types of anthropogenic input. Since the 1850s, fossil-fuel burning has introduced "old" carbon into the atmosphere, thereby lowering the $^{14}C/C$ of CO_2. This is called the **Suess Effect**. The second input has been the result of ^{14}C production during bomb testing.

For the purposes of comparison, all $^{14}C/C$ ratios are now reported as $\Delta^{14}C$. This is essentially the difference (in parts per thousand, or "per mil") between

a sample's $^{14}C/C$ and the ratio that was present in atmospheric CO_2 prior to the onset of these anthropogenic inputs. Since fossil-fuel burning lowers the atmospheric $^{14}C/C$, it has caused the $\Delta^{14}C$ of CO_2 to become negative. This change in isotopic composition has been recorded in trees that deposit atmospheric carbon in annual rings. Since these rings are datable, their relative radiocarbon content can be reported as a function of time, as shown in Figure 28.20. Fluctuations prior to 1850 were probably caused by changes in sunspot activity and in the strength of Earth's magnetic field, both of which affect the atmospheric flux of cosmic rays.

The relative radiocarbon content of coral reefs has also been used as a long-term record of changes in $\Delta^{14}C$. As a result of seasonal changes in growth rates, coral also deposit carbon in datable layers. But coral deposit carbon derived from surface-water DIC, so the radiocarbon composition of their calcium carbonate is not directly related to that which was concurrently present in the atmosphere. As shown in Figure 28.21, the radiocarbon content of newly deposited coral carbonate was relatively constant until the 1950s. At this time, a massive increase in the amount of ^{14}C occurred as a result of aboveground atomic bomb testing. This input declined abruptly in the 1960s as a result of the implementation of an international test ban. The input of radiocarbon was so large that it swamped the Suess Effect.

In the Northern Hemisphere, the anthropogenic input has increased the radiocarbon inventory by 50 percent. Unlike the Suess Effect, this addition of radiocarbon represents only a temporary perturbation as most will eventually be lost to decay. Thus radiocarbon ages of materials formed after 1950 will have to be corrected for the declining presence of this bomb-derived ^{14}C.

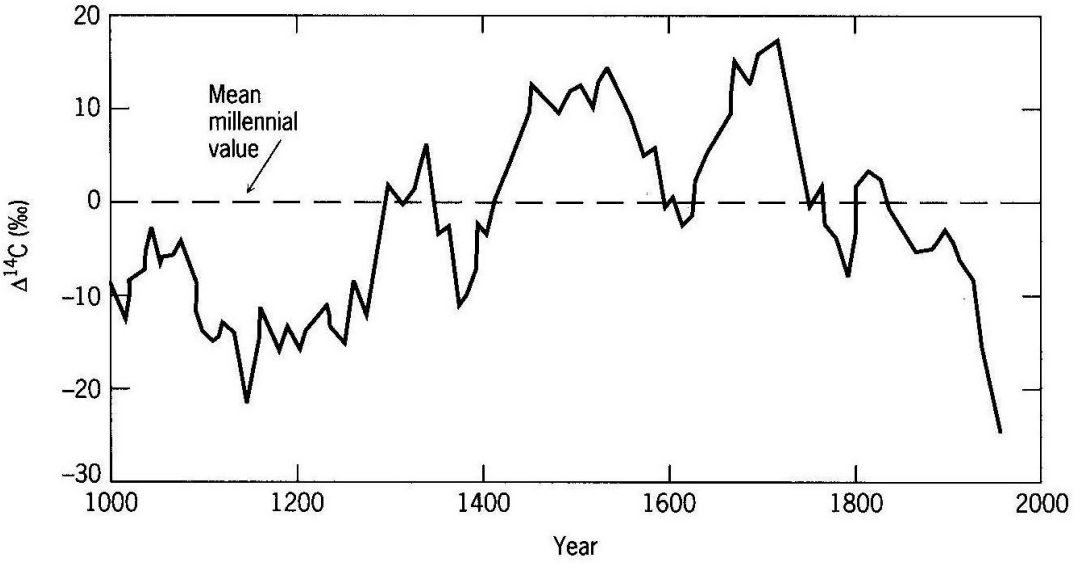

FIGURE 28.20. $^{14}C/C$ ratio (expressed as $\Delta^{14}C$) for atmospheric CO_2 over the last 1000 y as reconstructed from tree ring measurements. *Source*: From M. Stuiver and P. D. Quay, reprinted with permission from *Earth and Planetary Science Letters*, vol. 53, p. 354, copyright © 1981 by Elsevier Science Publishers, Amsterdam, The Netherlands.

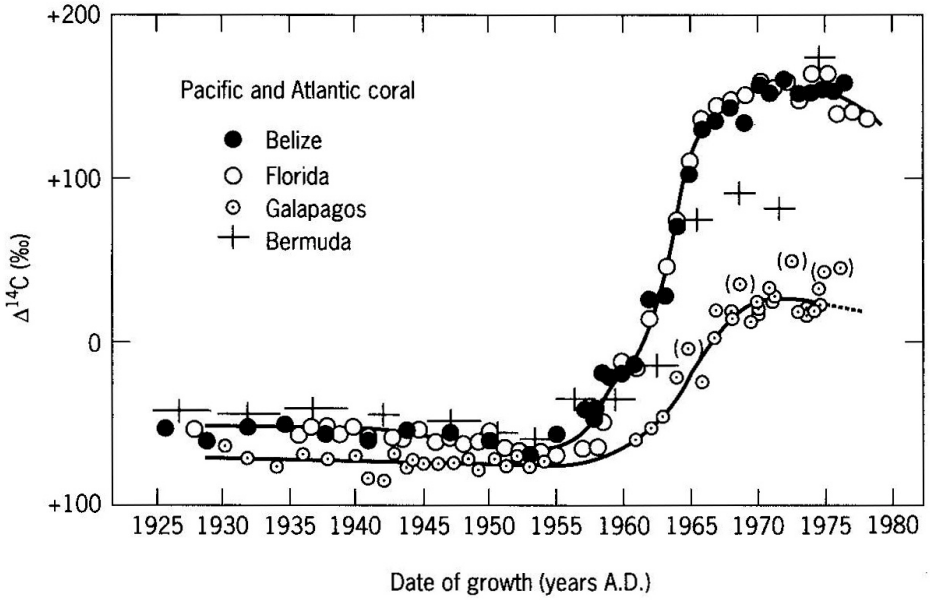

FIGURE 28.21. $\Delta^{14}C$ values obtained from corals. The Galapagos coral comes from an area of intense upwelling in the western equatorial Atlantic that has evidently supplied a significant amount of nonradiogenic DIC to the coral. *Source*: From E. M. Druffel and H. E. Suess, reprinted with permission from the *Journal of Geophysical Research*, vol. 88, p. 1273, copyright © 1983 by the American Geophysical Union, Washington, DC.

The coral isotope record has been used to estimate what the $^{14}C/C$ of DIC must have been prior to the testing of atomic bombs and the onset of the Suess Effect. This preindustrial value has been used to correct deep-water radiocarbon concentrations for atomic bomb and fossil-fuel contamination. As shown in Figure 28.22, the resultant deep-water distribution of radiocarbon is consistent with that of other water-mass tracers.

Some ^{14}C-labeled POC is transported to the seafloor. The radiocarbon content of this sedimentary organic matter can be used to determine sedimentation rates. Due to ^{14}C's relatively short half-life, this isotope is only of use in rapidly accumulating sediments. An example is given in Figure 28.23, where radiocarbon measurements have been converted to "ages."

The change in slope at mid depth in these cores is interpreted as the result of a change in sedimentation rate. The timing of the shift is coincident with the end of the last ice age. This suggests that rising sea level has reduced the rate at which sediment is supplied to this ocean site, probably by pushing the coastline inshore. Such records of changes in sedimentation rate are an important source of information regarding climate and other features of the crustal-ocean factory.

Bioturbation has homogenized the radiocarbon distributions in the top 10 cm of these cores, causing their surface sediments to have a constant "age." The absence of a radiocarbon gradient can be used to assess the depth to which bioturbation mixes the surface sediments. These data can also be used to infer

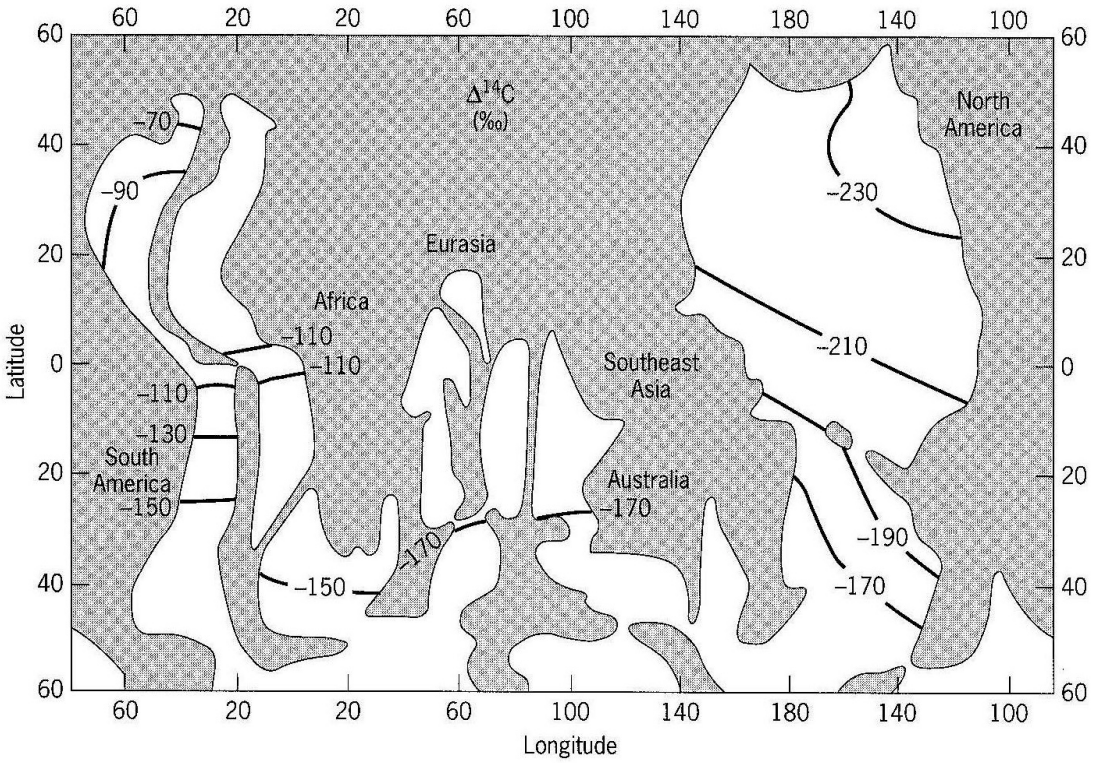

FIGURE 28.22. Distribution of $\Delta^{14}C$ at a depth of 4000 m in the main ocean basins. *Source*: From *Tracers in the Sea*, W. S. Broecker and T.-H. Peng, copyright © 1982 by the Lamont-Doherty Geological Observatory, Palisades, NY, p. 248. Reprinted by permission. Data from H. Stuiver and H. G. Östlund, reprinted with permission from *Radiocarbon*, vol. 22, p. 5, copyright © 1980 by the University of Arizona, Department of Geosciences, Tucson, AZ; H. G. Östlund and H. Stuiver, reprinted with permission from *Radiocarbon*, vol. 22, p. 29, copyright © 1980 by the University of Arizona, Department of Geosciences, Tucson, AZ, and H. G. Östlund, R. Oleson and R. Brescher, *Tritium Laboratory Data Report #9*, 1980, Rosenstiel School of Marine and Atmospheric Science, University of Miami, Miami, FL. Reprinted by permission.

bioturbation rates. On the other hand, this vertical transport of radiocarbon limits the resolution to which each sediment layer can be dated.

ARTIFICIAL RADIONUCLIDES

A large amount and great variety of radionuclides have been introduced into the marine environment as a result of human activities. The radioactivity of these isotopes is usually reported in picocuries (pCi). One Ci is equal to 2.200×10^{12} dpm, which is equivalent to the activity of 1 g of radium. Thus 1 pCi is equal to 2.200 dpm. Fallout from the testing of atomic bombs and intentional leakage from nuclear reactors are the two major sources of the artificial radionuclides now present in the ocean. The impact of nuclear reactors is discussed in Chapter 30.

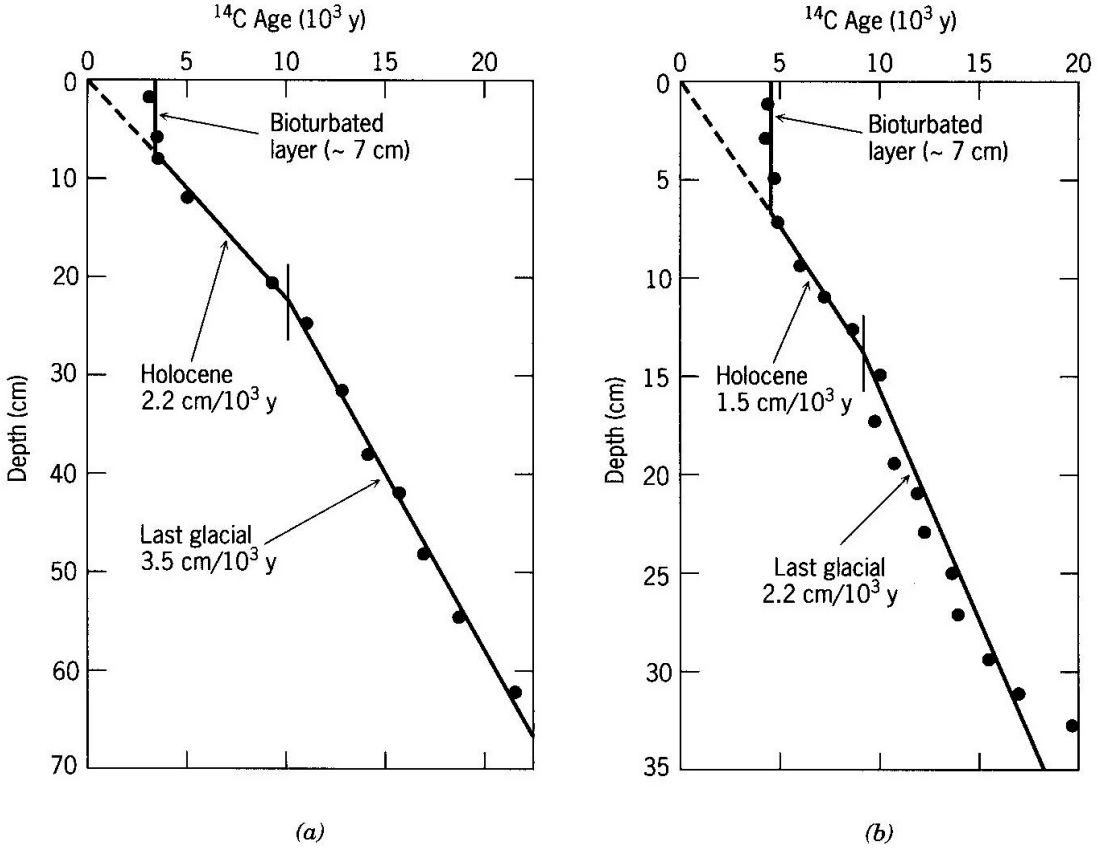

FIGURE 28.23. Radiocarbon ages as a function of depth in a deep-sea core from (*a*) the Indian Ocean (7°N 61°E) and (*b*) the Pacific Ocean (2°S 157°E). *Source*: From *Tracers in the Sea*, W. S. Broecker and T.-H. Peng, copyright © 1982 by the Lamont-Doherty Geological Observatory, Palisades, NY, p. 258. Reprinted by permission. Data from (*a*) *The Fate of Fossil Fuel CO_2 in the Ocean*, T.-H. Peng, W. S. Broecker, G. Kipphut, and N. Shackleton (eds.: N. Andersen and A. Malahoff), copyright © 1977 by Plenum Press, NY, p. 357 (reprinted by permission); (*b*) T.-H. Peng, W. S. Broecker, and W. H. Berger, reprinted with permission from *Quaternary Research*, vol. 11, p. 143, copyright © 1979 by Academic Press, Orlando, FL.

During the explosion of atomic bombs, radionuclides are produced directly by fission. High-energy neutrons are also produced. Some of these neutrons collide with the metallic bomb casings, earth, water, and atmospheric gases, thereby producing other **artificial radionuclides**. This process is termed neutron activation. In the first weeks after an explosion, radioactive decay is dominated by the short-lived radionuclides, such as ^{143}Pr, ^{140}Ba, ^{147}Nd, and ^{131}Ir. After 20 y, most of these isotopes have decayed, leaving ^{90}Sr and ^{137}Cs as the most abundant radionuclides. Other artificial radionuclides that are present in the marine environment are listed in Table 28.7. As indicated, some become strongly enriched in the tissues of marine organisms, much like the naturally occurring trace metals.

As shown in Figure 28.24, most of the aboveground bomb testing was done between 1958 and 1965 in the Northern Hemisphere. (The USA, USSR, and

TABLE 28.7
The Most Abundant Artificial Radionuclides in the Marine Environment[a]

Symbol	Element	Half-life	Radiation Type	Enrichment Factor	
				Mollusk	Fish
1. Fission products in nuclear reactions					
^{3}H	Tritium	12.3	β		
^{14}C	Carbon–14	5680	β		
^{85}Kr	Krypton–85	10.6	β	1	1
^{89}Sr	Strontium–89	0.14	β	1	0.2
^{90}Sr	Strontium–90	28.0	β	1	0.2
^{90}Y	Yttrium–90	0.007	β	15	10
^{91}Y	Yttrium–91	0.16	β	15	10
^{95}Nb	Niobium–95	0.10	β–γ	5	1
^{95}Zr	Zirconium–95	0.18	β–γ	5	1
^{103}Ru	Ruthenium–103	0.11	β-γ	10	1
^{106}Ru	Ruthenium–106	1.0	β–γ	10	1
^{131}I	Iodine–131	0.02	β–γ	50	10
^{137}Cs	Cesium–137	30.0	β–γ	10	10
^{144}Ce	Cerium–144	0.78	β–γ	400	3
2. Activation products					
^{32}P	Phosphorus–32	0.04	β	6000	3300
^{51}Cr	Chromium–51	0.08	K–γ	400	100
^{54}Mn	Manganese–54	0.86	K–γ	10,000	200
^{55}Fe	Iron–55	2.7	K	10,000	1500
^{57}Co	Cobalt–57	0.74	K–γ	500	80
^{60}Co	Cobalt–60	5.3	β–γ	500	80
^{65}Zn	Zinc–65	0.67	K–β–γ	10,000	1000
^{110}Ag	Silver–110	0.69	β–γ	10,000	—
^{134}Cs	Cesium–134	2.1	β–γ	10	10

Source: From *Marine Pollution, Diagnosis and Therapy*, S. A. Gerlach, copyright © 1981 by Springer-Verlag, Heidelberg, Germany, p. 108. Enrichment data from *Impingement of Man on the Oceans*, T. R. Rice and D. A. Wolfe (ed.: D. W. Hood), copyright © 1971 by John Wiley & Sons, Inc., New York, p. 351. Reprinted by permission.

[a]Their half-lives are listed in years. K emitters are radionuclides that generate gamma rays (γ) as a result of electron capture. The enrichment factors are given with respect to wet weight.

UK signed a test ban treaty in 1962.) Depending on the location of the bomb test, some radionuclides were introduced directly into the ocean; others were deposited on land or injected into the atmosphere. Wind mixing spread the atmospheric input across the globe. Eventually most of these radionuclides were deposited as fallout, either on the sea surface or land. Some of the radionuclides deposited on land were eventually transported to the ocean via river and groundwater runoff.

As is evident from Figure 28.24, the production and deposition of artificial radionuclides has been carefully monitored. Since the input rates of these

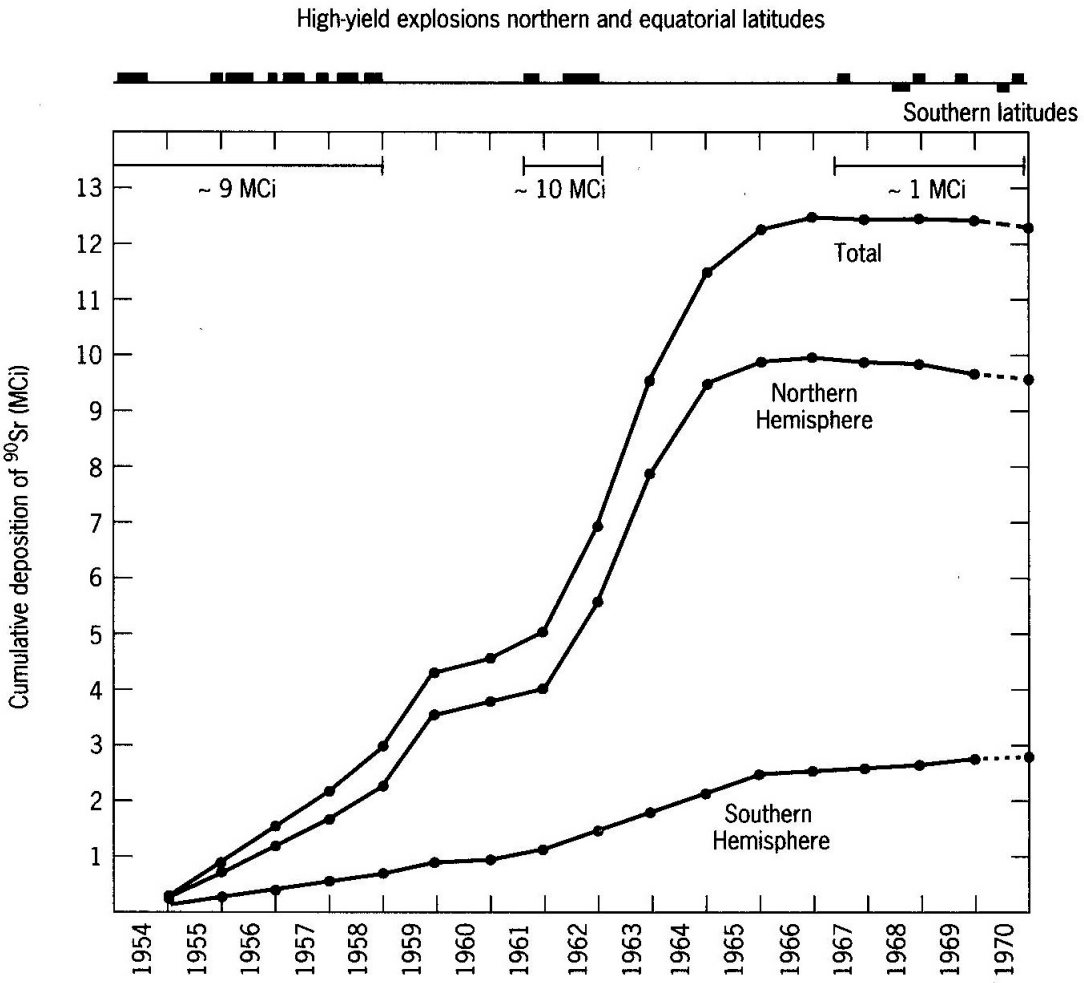

FIGURE 28.24. Cumulative deposition of ^{90}Sr in MCi (10^3 Ci). *Source*: From D. H. Pierson, reprinted with permission from *Nature*, vol. 234, p. 80, copyright © 1971 by Macmillian Journals, Ltd., London, England.

isotopes are very well known, they make excellent water-mass tracers. In particular, marine distributions of bomb-derived ^{90}Sr, tritium, and radiocarbon have been used to infer rates of water motion. Some of these applications are discussed below.

By the early 1970s, little of the bomb-derived ^{90}Sr had penetrated below the mixed layer as a result of mixing, at least at low and mid latitudes, as shown in Figure 28.25. The transport that had occurred at these sites was primarily the result of particle scavenging and incorporation into biogenic particles. At subpolar latitudes, the thermocline is weak and hence mixing would be expected to have caused a deeper injection of the artificial radionuclides. This has been observed for tritium, as described below.

Upon injection into the atmosphere, bomb-derived **tritium** was rapidly incorporated into gaseous water molecules. This caused rainwater to have very high tritium levels during the early 1960s (Figure 28.26). Thus bomb testing in the 1950s and 1960s caused anthropogenic tritium to be introduced into the ocean as a rapid, short-lived injection that was concentrated in the Northern

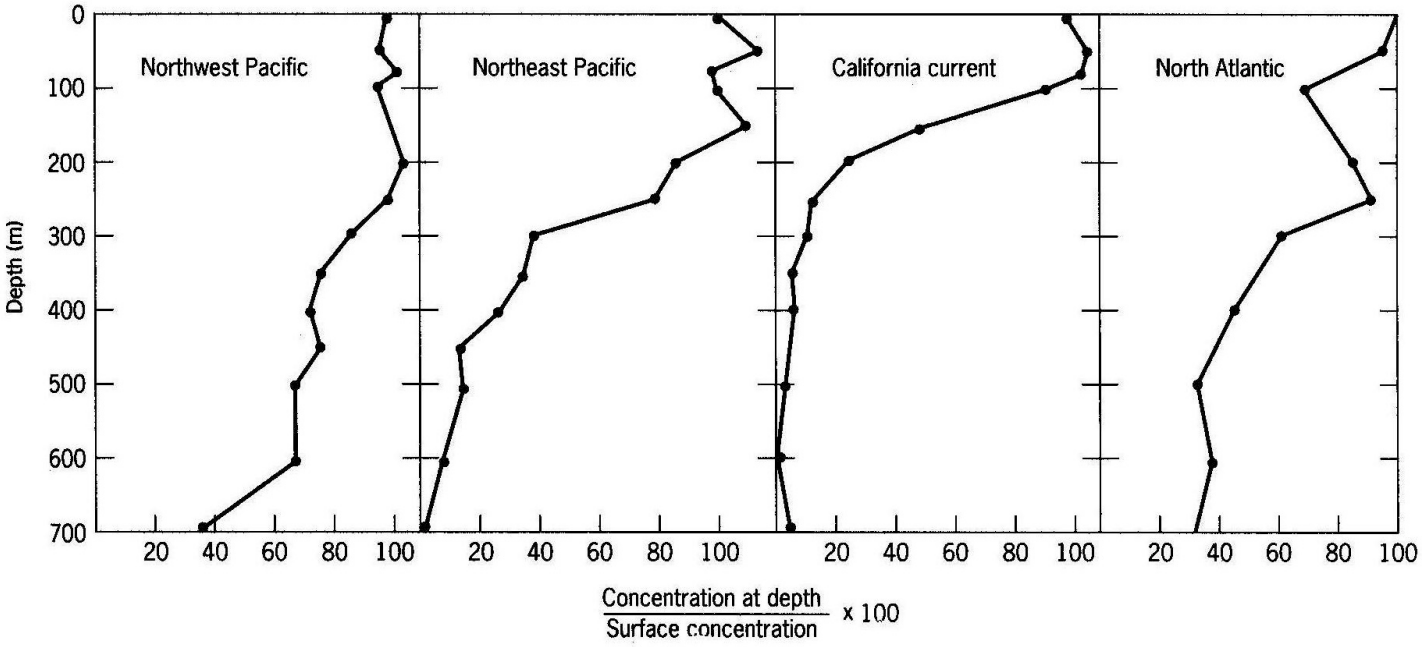

FIGURE 28.25. ^{90}Sr concentrations in the Atlantic and Pacific oceans given as the percentage of surface-water concentrations. *Source*: From *Radioactivity in the Marine Environment*, H. L. Volchok, V. T. Bowen, T. R. Folsom, W. S. Broecker, E. A. Schubert, and G. S. Bien (ed.: National Research Council), copyright © 1971 by the National Academy of Science, Washington, DC, p. 25. Reprinted by permission.

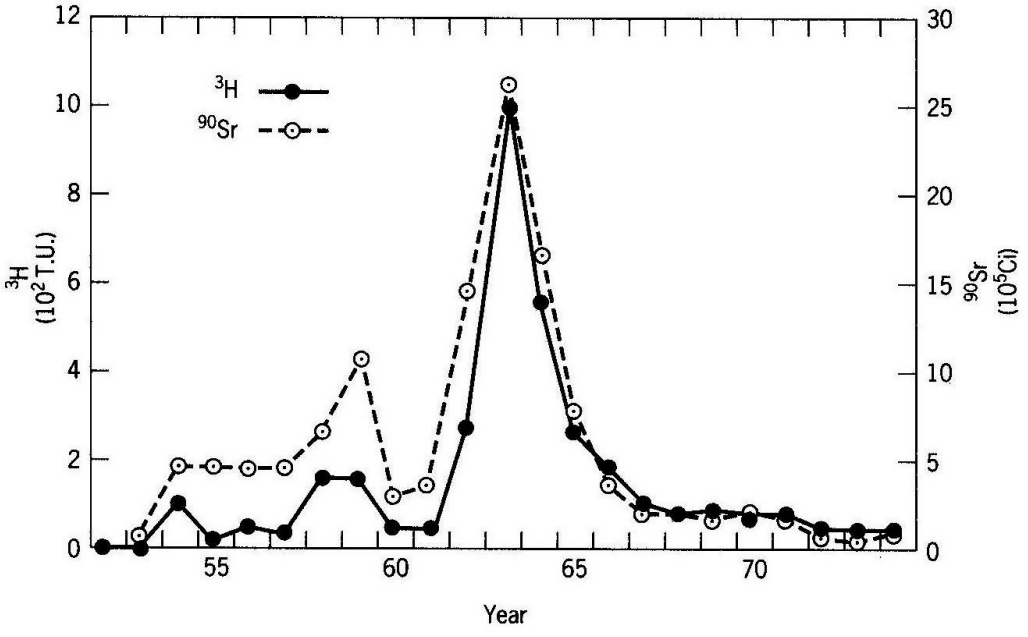

FIGURE 28.26. Plot of the ^3H content of rain at the west coast of Ireland, from 1952 to 1974 (solid circles). Tritium levels are reported in tritium units (T.U.), which are equal to $10^{18} \times (^3H/^1H)$. Also given is the total annual northern hemisphere ^{90}Sr deposition (open circles) in 10^5 Ci. *Source*: From E. Dreisigacker and W. Roether, reprinted with permission from *Earth and Planetary Science Letters*, vol. 38, p. 307, copyright © 1978 by Elsevier Science Publishers, Amsterdam, The Netherlands.

Hemisphere. The nature of this injection has made tritium a very useful tracer of water-mass motion. Since its half-life is only 12.5 y, much of the anthropogenic tritium has already decayed. Due to its rapidly decreasing activity, bomb-derived tritium will be usable as a tracer only for a few decades.

As shown in Figure 28.27, the penetration of anthropogenic tritium into the ocean has also been restricted to the mixed layer at low and mid latitudes. In contrast, tritiated water has already reached a water depth of 2 km in the subpolar North Atlantic. This is likely due to the formation of NADW via the sinking of surface waters at high latitudes. Although a small amount of tritium is produced by spallation in the atmosphere, rapid decay causes natural levels to be quite low.

This tritiated water has been followed as a coherent advective flow as far south as Florida. As shown in Figure 28.28, this deep-water current flows along the seafloor of the North Atlantic's western margin. It is thought to be

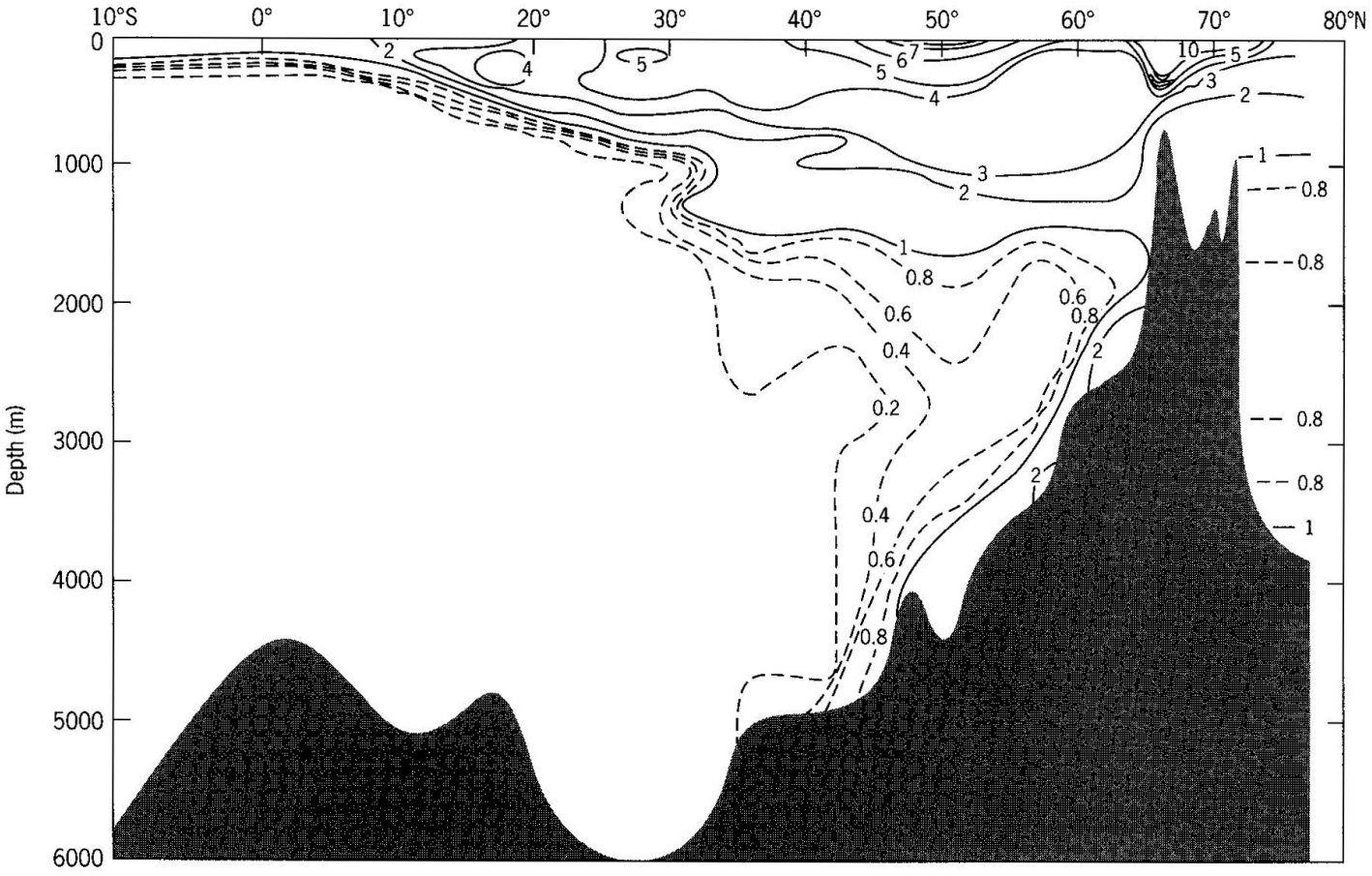

FIGURE 28.27. Distribution of tritium in (T.U.) in the western Atlantic Ocean. (See Figure 28.26 for unit definition.) This diagram indicates the extent to which bomb-produced material has penetrated the deep ocean over a period of about 10 y. *Source*: From H. G. Östlund and C. G. H. Rooth, reprinted with permission from the *Journal of Geophysical Research*, vol. 95, p. 20154, copyright © 1990 by the American Geophysical Union, Washington, DC.

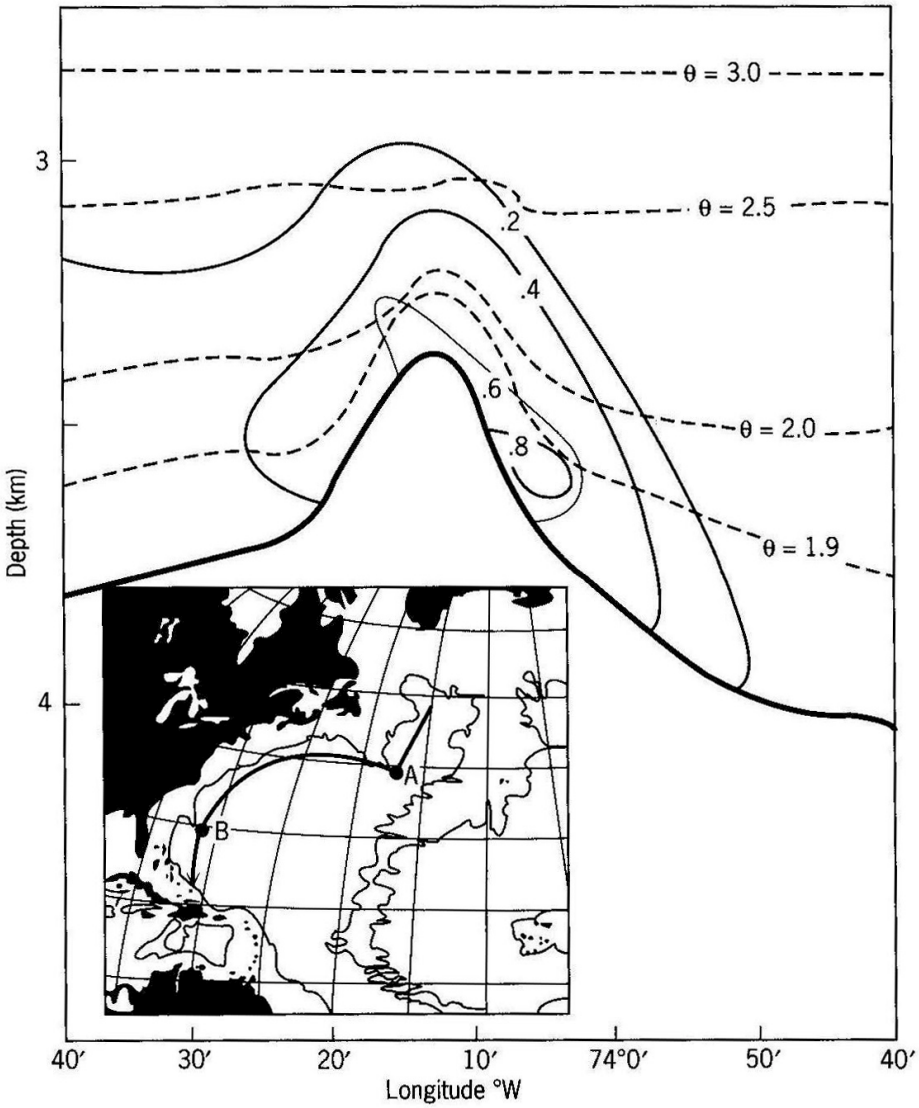

FIGURE 28.28. Cross-sectional tritium profile through bottom waters flowing along the Blake-Bahama Outer Rise. The site location is identified on the inset map as B. The solid contours are the relative tritium abundances in T.U.s (see Figure 28.26 for unit definition) and the dashed contours are for potential temperature. *Source*: From *Tracers in the Sea*, W. S. Broecker and T.-H. Peng, copyright © 1982 by the Lamont-Doherty Geological Observatory, Palisades, NY, p. 411. Reprinted by permission. Data from W. J. Jenkins and P. B. Rhines, reprinted with permission from *Nature*, vol. 286, p. 879, copyright © 1980 by Macmillan Journals, Ltd., London, England.

responsible for the transport of sediment that has been deposited on the Blake-Bahama Outer Rise as the huge delta over which the current now flows.

Tritium distributions have been used to study mixing processes in the surface waters and thermocline. For example, turnover times for the mixed layer and thermocline have been inferred from the application of the one-dimensional advection-diffusion model presented in Chapter 4 to vertical profiles of ^3H, salinity, and temperature. The results for temperate latitudes are summarized in Figure 28.29 as ventilation ages. This is the length of time

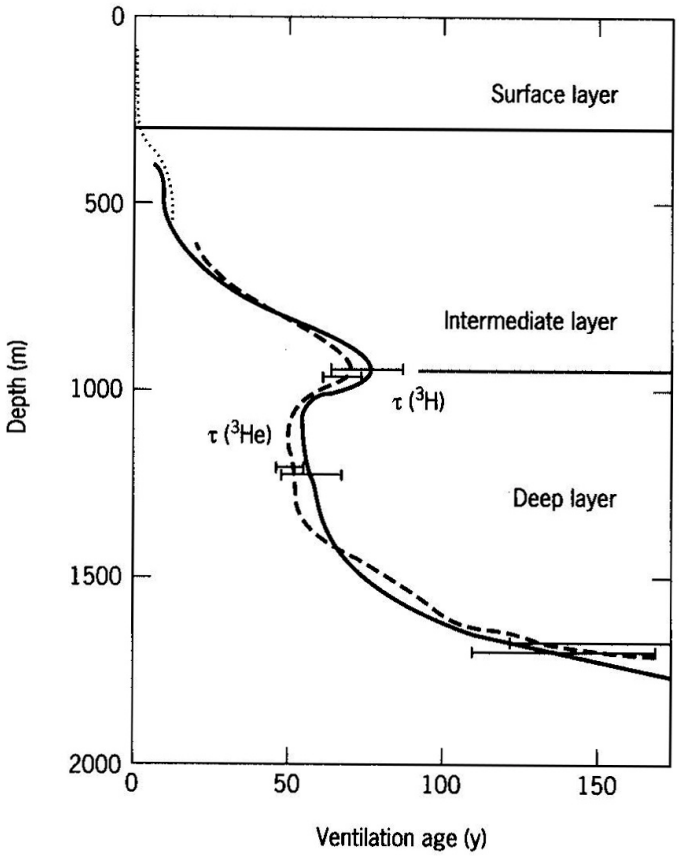

FIGURE 28.29. Ventilation ages of water inferred from tritium and ^{3}He distributions. The surface, intermediate, and deep layers are approximately analogous to the mixed layer, thermocline, and deep zone. *Source*: From *The Major Biogeochemical Cycles and Their Interactions*, M. E. Fiadeiro (eds.: B. Bolin and R. B. Cook), copyright © 1983 by John Wiley & Sons, Inc., New York, p. 464. Reprinted by permission. Data from W. J. Jenkins, reprinted with permission from the *Journal of Marine Research*, vol. 38, p. 599, copyright © 1979 by the Journal of Marine Research, New Haven, CT.

required for isopycnal processes to completely replace the water located at a particular depth. These processes are thought to involve convective overturn during the winter, followed by horizontal transport, as shown in Figure 28.30. Since the water masses start their journey at the sea surface, they are rich in atmospheric gases. Isopycnal transport carries this gas below the sea surface and hence acts to "ventilate" the ocean.

From these results, the water column at temperate latitudes appears to be occupied by three different types of water. The surface layer, which occupies the top 50 m, has a tritium "age" of less than 1 y. Thus this water mass can be characterized as well mixed and highly variable in composition on short time scales. Below this, the ventilation age of the water masses increases with depth to 1000 m. This coincides with the base of thermocline, suggesting that the waters in this intermediate layer are relatively stagnant and isolated as a result of slower isopycnal advection and density stratification. The underlying

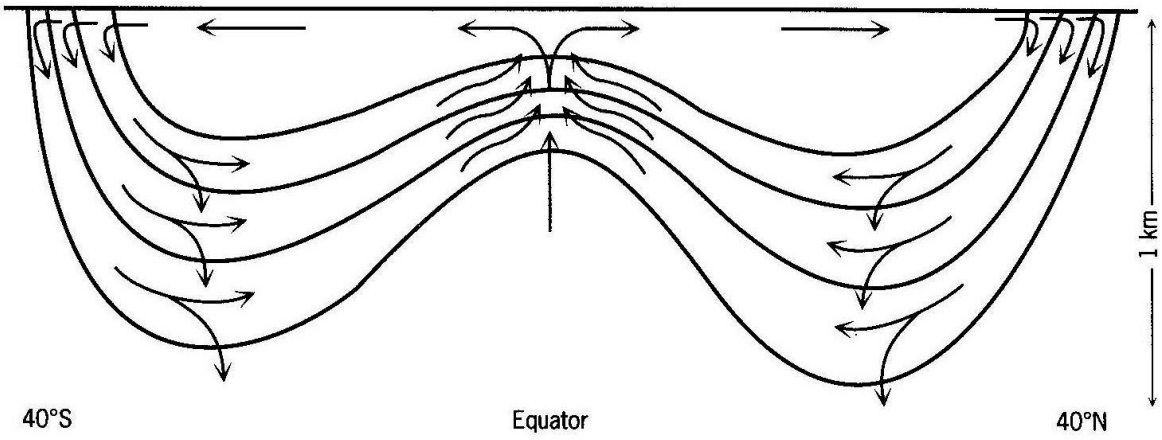

FIGURE 28.30. Isopycnal transport of water to depths below the sea surface. This process is thought to be responsible for the ventilation of the thermocline. *Source*: From *Tracers in the Sea*, W. S. Broecker and T.-H. Peng, copyright © 1982 by the Lamont-Doherty Geological Observatory, Palisades, NY, p. 440. Reprinted by permission.

water has a shorter ventilation age, reflecting the effects of relatively fast thermohaline-driven advection.

Due to its naturally high concentrations in seawater, bomb-derived radiocarbon does not make as "clean" a tracer of water-mass motion as tritium. Nevertheless, the pathway and degree of bomb radiocarbon penetration have also been used to validate ocean-mixing models. These models are presently being used to predict the fate of anthropogenic CO_2 in the ocean.

SUMMARY

Radioisotopes (or **radionuclides**) are atoms that spontaneously undergo nuclear transformations at a fixed rate and in doing so attain a greater measure of stability. **Radioactive decay** can occur through four types of nuclear reactions. If **protons** are in excess, stability is achieved either through emission of **α particles** ($^4_2$**He**) or **positrons** (β^+), or by **electron capture**. If **neutrons** are in excess, stability is achieved via the emission of β^- **particles**, which are high-energy **electrons** ($^0_{-1}e$).

The production rates of these high-energy particles are easily measured. They are functionally equivalent to the decay rate, or **activity**, of the parent radionuclide. Activities are usually reported as **disintegrations per minute (dpm)**. The activity of a radionuclide in a sample of seawater or sediment is reported in terms of dpm/L or dpm/g, respectively. These **specific activities** (A) are directly related to the concentration of the radionuclide by $A = \lambda[N]$, where λ is the **decay constant**. Thus the rate at which a radionuclide decays is directly proportional to its concentration. This decay rate is commonly expressed as the **radioactive decay law**: $\ln(N/N_o) = -\lambda t$ where N is the amount (e.g., grams or moles) of radionuclide N. Decay constants are usually given in

terms of a **half-life**, which is the time required for radioactive decay to remove half of an initial amount of radionuclide. It is equal to $0.693/\lambda$.

Marine radionuclides are classified according to their source. The **primordial radionuclides** are isotopes that have been part of Earth since its formation. Thus they decay at very slow rates. In comparison, their **daughters** have relatively short half-lives. In the absence of other processes, the rapid decay of the daughter relative to its **parent** will eventually cause the pair to attain **secular equilibrium** in which $A_D = A_P$. Fortunately for marine chemists, many primordial radionuclides and their daughters are not present in secular equilibrium in the ocean. This is largely due to rapid removal of the daughter by adsorption onto sinking particles or incorporation into biogenic materials. The degree of disequilibrium can be used to compute the daughters' net removal rates. Secular disequilibrium has also been used to determine sedimentation rates, nodule accretion rates, and rates of water motion. These results are best confirmed with those from other isotopes. In doing so, it is important to recognize that the results reflect the half-lives of the isotopes. That is, the apparent behavior of the processes being measured is dependent on the time scales over which it is being observed.

Cosmogenic radionuclides are formed by **spallation reactions** that occur in the atmosphere. In these nuclear reactions, gas nuclei are fragmented as a result of collisions with high-energy **cosmic rays. Radiocarbon** (^{14}C) is the most commonly used cosmogenic radionuclide. Its marine distributions have been used to measure rates of water motion, sedimentation, bioturbation, and the timing of changes in sea level. Radiocarbon concentrations are usually measured relative to the amount of total carbon present in a sample ($^{14}C/C$). The relative abundance of radiocarbon has been greatly altered as a result of the introduction of "dead" carbon from the burning of fossil fuel. This is called the **Suess Effect** and had caused $^{14}C/C$ ratios to decline until the 1950s. At this time, radiocarbon concentrations were greatly increased as a result of atomic bomb testing. This input has been so large that it has, at least temporarily, swamped the Suess Effect.

Bomb testing, as well as intentional leakage from nuclear reactors, has introduced other **artificial radionuclides** into the ocean. For example, the natural inventory of **tritium** has also been greatly elevated. Both tritium and bomb radiocarbon have been used to obtain much information about the rates of thermohaline circulation and the processes by which waters in the mixed layer and thermocline are renewed.